Continental Shelf Research 65 (2013) 121–140

Contents lists available at ScienceDirect

Continental Shelf Research

journal homepage: www.elsevier.com/locate/csr

Research papers

The seasonal circulation of the Eastern Brazilian shelf between 10°S and 16°S: A modelling approach

F.N. Amorim [a,*], M. Cirano [a,b], M. Marta-Almeida [a], J.F. Middleton [b], E.J.D. Campos [c]

[a] Grupo de Oceanografia Tropical, Inst. de Física, Universidade Federal da Bahia, Travessa Barão de Jeremoabo, s/n, 40170-280 Salvador, Bahia, Brazil
[b] Aquatic Sciences, South Australia Research and Development Institute, Adelaide, Australia
[c] Instituto Oceanográfico da Universidade de São Paulo, São Paulo, Brazil

ARTICLE INFO

Article history:
Received 22 October 2012
Received in revised form
3 June 2013
Accepted 6 June 2013
Available online 24 June 2013

Keywords:
Shelf currents
Wind-driven circulation
Western Boundary Currents
South Equatorial Current
Regional Modelling

ABSTRACT

The Regional Ocean Modelling System (ROMS) with embedded nesting capabilities based on AGRIF, configured with a refined grid (1/36°) and realistic forcings (6-hourly winds and surface fluxes, daily large scale oceanic forcings and tides), was implemented to describe the seasonal circulation within the Eastern Brazilian Shelf (EBS) between 10°S and 16°S and its interaction with the mesoscale dynamics associated with the Western Boundary Currents (WBC) which flow over the slope: the Brazil Current/North Brazil Current-Undercurrent (BC/NBC–NBUC), as well as the contribution of the forcing mechanisms on the generation of the shelf/slope currents. The model results show, based on the methodology adopted, that for the northern limit (10°S) the northward flow is the dominant pattern while the southward flow appears as a shallow flow confined to the top 50 m of the water column during the spring/summer seasons. The surface circulation at the inner- and mid-shelves in this region is mostly influenced by the wind forcing, while at the shelf-break the currents are mainly driven by the slope currents during all seasons. In the middle (14°S) and southern (16°S) domains, there is an alternate dominance of the southward/northward flows for the first 150 m of the water column, with the dominance of the southward (northward) flow between October–February (March–September) at 14°S. However, the annual net transport in these regions is oriented southwards. On the other hand, in the sub-surface (~150–400 m) the dominance of the northward flow is clear. At 14°S, the inner-shelf circulation is mainly driven by the wind forcing and the mid-shelf circulation is forced by both the wind and the flow over the slope, while the currents at the shelf-break are more influenced by the currents at the slope. Finally, the inner- and mid-shelf currents at 16°S are mainly driven by the wind forcing, while the shelf-break currents present a poor correlation with the wind and a strong influence of the WBC dynamics.

1. Introduction

The Eastern Brazilian Shelf (EBS), geographically located between 13°S and 22°S (Knoppers et al., 1999) and dynamically limited between 8°S and 15°S (Castro and Miranda, 1998), hosts the bifurcation of the southern branch of the South Equatorial Current (SEC). At its upper level, the bifurcation is associated to the origin of two major shelf/slope Western Boundary Currents (WBC): the poleward Brazil Current (BC) and the equatorward North Brazil Current/North Brazil Undercurrent (NBC/NBUC). The SEC is fed by the subduction of warm and salty waters from the subtropical Atlantic eastward circulation area, which is one of the zones in the South Atlantic Ocean of prime importance in global climate change (Stramma et al., 1990; Stramma and England, 1999). In addition, apart from the Abrolhos Bank (AbB) on its southern position, the EBS represents the narrowest continental shelf along the South American Eastern Coast, with a typical width of 15 km (Castro and Miranda, 1998) and only 8 km wide off Salvador city (Knoppers et al., 1999). This turns the EBS into a peculiar region in the world context, since such narrow shelves are not a common feature along passive continental margins.

The major portion of variability in the Tropical Atlantic currents is considered to be driven by large-scale seasonality in the trade wind regime and the latitude of the marine Inter-Tropical Convergence Zone (ITCZ) (Stramma and Schott, 1999). Following the north–south displacement of the ITCZ, the SEC bifurcation undergoes a seasonal latitudinal excursion which, according to Rodrigues et al. (2007), is strongest in the top 400 m, where it reaches a southernmost position (~17°S) in July and a northernmost position (~13°S) in November. In a mesoscale perspective, the near surface flow at the shelf/slope region of the SEC bifurcation is associated

* Corresponding author. Tel.: +55 27 99524192.
E-mail address: fnamorim@gmail.com (F.N. Amorim).

0278-4343/$ - see front matter © 2013 Elsevier Ltd. All rights reserved.
http://dx.doi.org/10.1016/j.csr.2013.06.008

with eddy structures. In an annual mean, between 15°S and 20°S, the BC could be interpreted as the flow composed by the coastal border of three robust anticyclones (Soutelino et al., 2011). It is well known that mesoscale processes related to WBC can influence the circulation in the outer-shelf region (e.g. Allen et al., 1983; Lee et al., 1984; Soares and Moller, 2001; Campos et al., 2000). In the EBS, however, these mesoscale features can also influence the mid-shelf region, leading to events of a complete reversal of the shelf currents (Amorim et al., 2011, 2012).

Locally, the shelf currents reflect the seasonal variation of the trade wind regime. During the austral autumn/winter seasons the circulation within the EBS is mainly driven by winds from SE to the north of ~20°S and experience a reversal of the preferential flow during the austral spring/summer seasons, when winds from E–NE prevails to the south of ~12°S (Dominguez, 2006; Amorim et al., 2011, 2012). Also, according to these authors, the passage of atmospheric frontal systems can cause episodic reversals of the preferential flow.

In addition to the complex hydrodynamics of the EBS described above, its topography also presents important features, such as the Salvador Canyon (SC), AbB and Royal-Charlotte Bank (RCB), which strongly affect the local circulation. Amorim et al. (2012), based on an original *in situ* dataset, showed that the surface circulation within the shelf adjacent to the SC (13°S), during the spring/summer seasons, is affected by a cyclone eddy formed by the interaction of the mean flow with the canyon topography, leading to an intensification of the wind upwelling system and enhancing the cross-shore exchanges. At the EBS southern region, the weakness of the BC flow over the extended and irregular shelf developed between the AbB (18°S) and RCB (16°S) leads to a strong interaction between the flow and topography which constrains and alters the flow, inducing a variability in the physical, chemical and biological features over the shelf and adjacent oceanic waters (Rezende et al., 2011; Soutelino et al., 2011).

Despite the complexity of the EBS circulation, the available literature is focused mainly on the large scale dynamics associated with SEC bifurcation and the associated WBC. For instance, the works of Rodrigues et al. (2007), Rezende et al. (2011) and Veleda et al. (2011), based on numerical modelling forced with climatological products, provided a first picture on the seasonality of the SEC bifurcation . Rezende et al. (2011), in particular, associated the WBC formation with the SEC divergence and its seasonal interaction with the slope currents. Based on *in situ* data, Soutelino et al. (2011) provided important information about the mesoscale processes related to the BC and NBC/NBUC formation, Veleda et al. (2011, 2012) and Schott et al. (2005) investigated the WBC dynamics to the north of 10°S and Amorim et al. (2011, 2012) described the seasonality of the shelf and slope circulation at the central part (around 14°S) of the EBS. However, these data are limited in time and space.

Based on the assumptions above, this work aims to fill in the gap that still exists in the literature about the interaction between the large scale atmospheric and oceanic processes with the circulation within the EBS. To accomplish this task, the use of a long term regional model simulation configured with a refined grid and realistic forcings is intended to: (i) describe the seasonal variation of the circulation at the shelf/slope region; (ii) investigate the importance of the forcing mechanisms (wind and WBC) to the seasonal circulation and (iii) evaluate the long-term results and grid design, so that an operational version of the model might be implemented in the near future.

The paper is then organized as follows: the main regional setting is presented in Section 2. The model configuration together with its validation is described in Section 3. The model results are presented in Section 4. Finally, Section 5 presents an integrated discussion of the results.

2. Regional setting

The domain adopted for the numerical modelling is limited between 8°S and 19°S (Fig. 1), encompassing the whole dynamically limit of the EBS, which presents typical conditions of a tropical passive margin dominated by WBC (Castro and Miranda, 1998). As the southern branch of the SEC enters the EBS margin, it bifurcates into two major Brazilian WBC, the southward BC and the northward NBC/NBUC. The BC flow is associated with the warm and salty Tropical Water (TW, $T > 20$°C and $S > 36$) at its upper level (first 100/150 m of the water column). As it flows southward the BC is strengthened and gets deeper, incorporating the upper thermocline water of the South Atlantic Central Water (SACW, 6°C $< T < 20$°C and $34.6 < S < 36$). However, in the region of study, the BC is a shallow and weak flow associated only with the TW water mass, since it incorporates the southward SACW flow near 22°S, due to the excursion of the SEC bifurcation with depth (Stramma and England, 1999; Silveira et al., 2000; Cirano et al., 2006). On the other hand, the NBC is characterized as an intense WBC and the dominant surface circulation pattern at the western Tropical Atlantic Ocean (Silveira et al., 1994). The NBUC is the component of the NBC system that, occupying the top 1000 m of the water column, flows along the NE coast of Brazil up to Cabo de São Roque (~5°S) (Schott et al., 1998). Due to this, the upper thermocline at the region of study, underneath the surface layer, always flows northward carried by the NBUC.

Although the annual mean position of the SEC bifurcation, in the top 100 m, is located at 14°S–16°S (Stramma and England, 1999; Rodrigues et al., 2007), it undergoes a strong meridional wind seasonal cycle, mainly caused by the north–south displacement of the marine ITCZ, which is stronger in the top 400 m (Rodrigues et al., 2007). As a result, in the 15°S–20°S latitudinal range, the circulation is dominated by vortical features of about 100 km in radius and it is not clear whether there is a continuous BC or simply a flow resulting from averaging a succession of counterclockwise eddy structures (Soutelino et al., 2011), which could be caused by either the topographical constraints (e.g. AbB and RCB) or geophysical instabilities created by the BC–NBUC

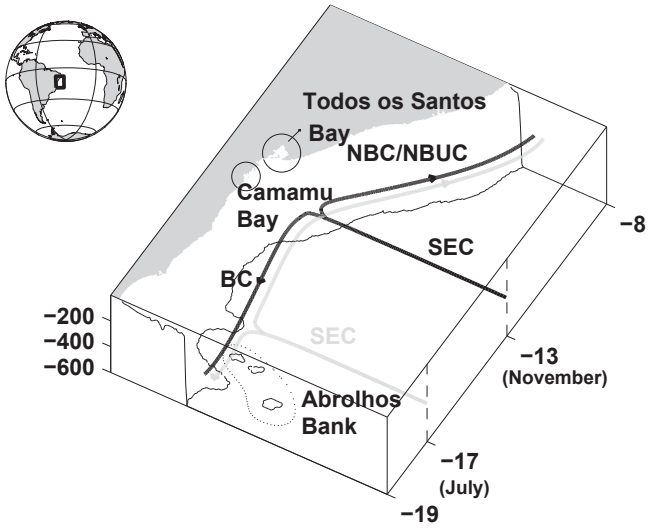

Fig. 1. Schematic seasonal variation of the Western Boundary Currents (WBC) at the upper levels along the Eastern Brazilian Shelf/slope region. The grey line shows the southernmost (17°S in July) position of the bifurcation of the South Equatorial Current (SEC), while the black line shows the northernmost position (13°S in November) of the bifurcation of the SEC according to Rodrigues et al. (2007). The poleward WBC is the Brazil Current (BC) while the equatorward WBC is the North Brazil Current/North Brazil Undercurrent System (NBC/NBUC). The locations of the important ecosystems are also shown. Modified from Amorim et al. (2011).

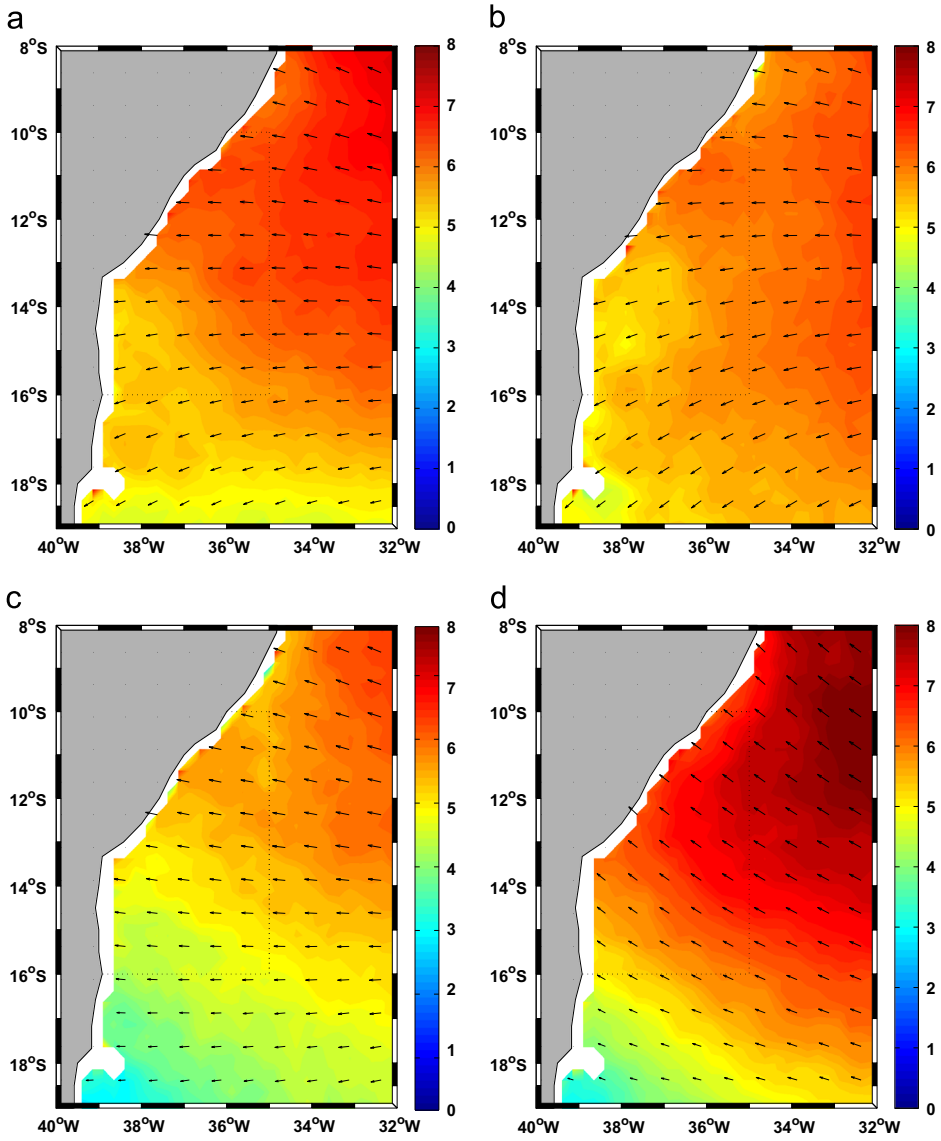

Fig. 2. Monthly mean (2004–2009) distribution of the winds at 10 m above the sea (vectors) derived from QuickSCAT (IFREMER, 2011), for the months of: (a) October, (b) January, (c) April and (d) July. The shaded area represents the wind intensity (m s^{-1}).

opposing flows, or a combination of both. Rezende et al. (2011), based on numerical modelling, argue that between 13°S and 16°S there is a seasonal transition of the dominance of the NBUC (April to September) and BC (October to March) flows, while between 8°S and 13°S (16°S–20°S) the NBUC (BC) flow is the dominant pattern.

Regarding the seasonality of the shelf currents along the EBS, Amorim et al. (2011, 2012) show that the currents at the shelf (13°S–14°S) are mainly wind-driven, experiencing a complete reversal of the mean flow between seasons, following a similar change in the wind field (Fig. 2). These authors also demonstrate that during the spring/summer seasons, the arrival of cold frontal systems is able to cause periodical reversals of the depth-integrated flow.

The shelf currents along the EBS are also influenced by topographic changes and tides. While Amorim et al. (2012) have shown that the presence of abrupt changes in topography enhance the upwelling system during spring/summer, Amorim et al. (2011) have found that the tidal circulation influence is of secondary importance. According to these authors, the generation of tidal currents account, at the near surface, for up to 31% and 22% of the variability of the cross-shore and alongshore currents, respectively. In addition, Pereira et al. (2005), studying the internal tides, have also found that the region around 14°S is the least affected by these oscillations.

Ecologically speaking, the EBS extension (Fig. 1) is occupied by important ecosystems and a great diversity of coral fauna at the mid- and outer-shelf regions (Olavo et al., 2011). The Todos os Santos Bay, located at the northern part of the domain, is affected by intensive industrial, commercial and fishing activities (Lessa et al., 2001). At its central portion, the Camamu Bay is still considered a pristine ecosystem and an important niche for the local artisan fishing and tourism. Finally, the AbB located at the southern portion of the EBS hosts the most extensive coral reef aggregation of the South Atlantic Ocean (Leão, 2002).

3. Model setup

The ocean simulations were performed with the Regional Circulation Model (RCM) ROMS (*Regional Ocean Modelling System*), described in Shchepetkin and McWilliams (2003, 2005), with

embedded nesting capabilities based on AGRIF (*Adaptive Grid Refinement in Fortran*) described in Penven et al. (2006). ROMS is a 3D model that solves the free-surface, hydrostatic, primitive equations of the ocean over a variable topography (Shchepetkin and McWilliams, 2005; Haidvogel et al., 2008). The model adopts the orthogonal curvilinear coordinates in the horizontal and the stretched terrain-following coordinates in the vertical. It is the successor of SCRUM (*S-coordinate Rutgers University Model*), including improvements like high-order advection schemes, several sub-grid scale parametrizations, accurate pressure gradient calculation, radiation boundary layer and data assimilation. For computational economy, the hydrostatic primitive equations for momentum are solved using a split-explicit time stepping scheme which requires a special treatment and coupling between barotropic (fast) and baroclinic (slow) modes. Currently, all 2D and 3D equations are time discretized using a third order accurate predictor (Leap-Frog) and corrector (Adams-Molton) time-stepping algorithm which is very robust and stable. The enhanced stability of the scheme allows larger time-steps.

The regional grid adopted in this study (Fig. 3) has a horizontal resolution of 1/36° in both the meridional and zonal directions, covering the region between 8°S–19°S and 32°W–40°W (a total length of ~1222 km × 889 km). A 32 s-level resolution is adopted in the vertical, with 15 s-levels (top 200m of the water column) and 21 s-levels (top 500m of the water column) at the slope region, where the mean depth is 2000 m.

The RCM was nested into the Global Circulation Model (GCM) HYCOM (*HYbrid Coordinate Ocean Model*, version 2.2) coupled on the *Navy Coupled Ocean Data Assimilation*-NCODA system analysis (HYCOM, 2011), which provided the initial and daily boundary conditions (temperature, salinity, elevation and velocities). The horizontal resolution of the GCM is 1/12°. The elevation and 2D velocity are imposed at the open boundaries as a Chapman (1985) and Flather (1976) boundary conditions, respectively. The radiative boundary condition described by Marchesiello et al. (2001) is applied to the tracers and 3D velocity. In addition to the boundary conditions mentioned above, the model temperature, salinity and velocity (2D and 3D) were also nudged towards the HYCOM/NCODA daily values with a spatially variable relaxation time scale. At the open boundaries, the relaxation time scale ($1/c_j$) was defined as $\tau = 1/3$ days (8 h), while for the other grid points, an increasing relaxation time scale was given by

$$c_j = \frac{1}{2\tau}\left[1 + \cos\left(\frac{j\pi}{n}\right)\right] \quad \text{for } j \le n,$$
$$c_j = 0 \quad \text{elsewhere} \tag{1}$$

where the index j represents the distance from the open boundary in model grid points and the width of the relaxation zone (n) was 10 grid points. Barth et al. (2008); Zhang et al. (2012) and Marta-Almeida et al. (2013), obtained a better representation of the offshore features with the adoption of this procedure.

The surface boundary fluxes (humidity, pressure, temperature, precipitation and radiation) were based on the 6-hourly NCEP Reanalysis-2 (Kanamitsu et al., 2002), with a horizontal resolution of 1.8° (192 × 94 Gaussian grid points or approximately 200 km horizontal spacing). The surface wind stress and intensity were derived from the CERSAT/IFREMER (IFREMER, 2011), which provides the wind data from the QuikSCAT scatterometer and SSM/I radiometer. These data are projected in a regular grid, with a 0.25° spacial resolution and 6-hourly temporal resolution, using an objective mapping technique (kriging). The fluxes derived from these data are calculated internally by the RCM through the bulk formulation.

The RCM was also forced with tidal forcings from TPXO (*OSU TOPEX/Poseidon Global Inverse Solution*; Egbert and Erofeeva, 2002), which provides amplitudes and phases of the sea surface elevation and barotropic currents for eight main diurnal and semi-diurnal tidal components (K_1, O_1, P_1, Q_1 and M_2, S_2, N_2, K_2, respectively) and for two long period tidal components (M_f, M_m), with a spacial resolution of 1/4°.

The bottom topography was interpolated from GLOBE Task Team (1999), with a horizontal resolution of 1 km. The bathymetry, where necessary, was smoothed to fit bathymetric gradients to a maximum slope factor ($r = (h_{+1/2} - h_{-1/2})/(h_{+1/2} + h_{-1/2}) \sim 0.2$) in order to prevent pressure gradient errors associated with the sigma coordinate system (Haidvogel and Beckmann, 1999). Table 1 summarizes the RCM configuration.

The integration period of the RCM was six years, from January 1st/2004 to December 31st/2009. The first two years represent the

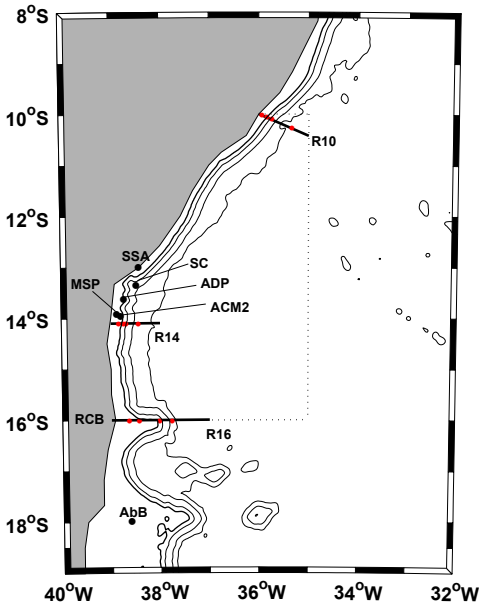

Fig. 3. The geographical domain covered by ROMS. The area inside the dotted lines represents the region of study. The three radials (black lines perpendicular to the coastline) at 10°S, 14°S and 16°S named R10, R14 and R16, respectively, are used to evaluate the seasonal hydrodynamics along the water column. Current time series at the inner-, mid- and outer-shelves and at the slope are evaluated for each radial (red dots). The main topographic features are represented by the Salvador Canyon (SC), the Royal-Charlotte Bank (RCB) and the Abrolhos Bank (AbB). Tidal data from FEMAR (2011) are available for the AbB, Morro de São Paulo (MSP) and Salvador (SSA) sites. The isobaths of 200 m, 1000 m and 3000 m are represented by light black lines. The shelf break is represented by the 70 m isobath (bold black line). (For interpretation of the references to colour in this figure caption, the reader is referred to the web version of this article.)

Table 1
Regional Circulation Model (RCM) setup parameters.

L	289	Number of points E–W
M	409	Number of points N–S
N	32	Number of *s*-levels
h_{max}	5000 m	Maximum region depth
h_{min}	5 m	Minimum region depth
θ_s	4	*S*-coordinates surface control parameter
θ_b	0	*S*-coordinates bottom control parameter
h_c	5 m	Typical width of the surface mixed layer depth
Δx	~3 km	Resolution in the zonal direction
Δy	~3 km	Resolution in the meridional direction
Δt	300 s	Baroclinic time step
Δt_f	300/45 s	Barotropic time step
r	3×10^{-4} m s^{-1}	Linear bottom drag coefficient
μ	30×10^{-3} m^2 s^{-1}	Viscosity coefficient in the relaxation layer
n	30 km	Width of the relaxation layer

model spin-up and, with the exception of tides, includes all forcings described above. The tidal forcing was introduced after the year of 2006. The period of analysis encompasses the years from 2006 to 2009, where the seasonal and space-temporal characterization of the circulation within the region of study is performed.

Table 2
Amplitude and phase (related to Greenwich) for the main tidal components derived from FEMAR (2011) and calculated from the RCM sea surface height time series (2006–2009). The phases from FEMAR are corrected for the Greenwich meridian. Units for amplitude and phase are cm and degrees, respectively.

Tidal component	FEMAR (Amp/Pha)	RCM (Amp/Pha)	Error (%) (Amp/Pha)
Salvador Station (12.97°S; 38.52°W)			
M_2	78.0/197	87.3/218	12/11
S_2	30.5/214	30.1/237	−1/10
O_1	6.6/164	7.4/167	12/2
K_1	4.1/260	5.3/252	29/–
Morro de Sao Paulo Station (13.90°S; 38.97°W)			
M_2	69.8/191	62.9/191	−10/0
S_2	25.1/207	23.9/207	−5/0
O_1	6.5/160	6.3/160	−3/0
K_1	4.3/249	4.0/245	−7/−2
Abrolhos Station (oceanic) (17.96°S; 38.70°W)			
M_2	78.4/189	79.4/191	1/1
S_2	33.1/209	32.7/207	−1/−1
O_1	7.8/165	8.0/152	2/−8
K_1	4.4/227	4.5/230	2/1

3.1. Model validation approach

In order to evaluate the RCM results prior to the analysis presented in Section 4, several time series were selected at specific locations with the aim of comparing the modelled results with the available observations at both supra-inertial and sub-inertial frequencies.

The amplitudes and phases of the main semi-diurnal (M_2 and S_2) and diurnal (O_1 and K_1) tidal components, calculated from the RCM sea surface height time series (2006–2009) using the harmonic analysis from Pawlowicz et al. (2002) are compared with those provided by FEMAR (2011) for Salvador (SSA), Morro de São Paulo (MSP) and Abrolhos (AbB) sites (Fig. 3). The results are presented in Table 2. The comparisons are made based on the percentage of the absolute error between the modelled (M) and observed (O) values, according to the equation $error = [(M-O)/O]*100$. Based on to this relation, positive (negative) values represent an overestimation (underestimation) of the amplitude/phase values of the RCM.

Overall, the RCM was able to reproduce the tidal sea surface height modulation with a tendency to overestimate the observed values, with the exception of the MSP site, where the RCM underestimates all the FEMAR data. For SSA and MSP sites, the error was under 15% (with the exception of K_1 component for SSA site). The smallest errors were observed at the AbB site, with values very close to the observed data. This behaviour could be attributed to the oceanic location of this station, which decreases the influence of bottom friction on tidal modulation.

For the circulation, our primary goal was to capture the seasonality of the currents both at the shelf and shelf/slope region. For the shelf region, we have chosen two points located at central

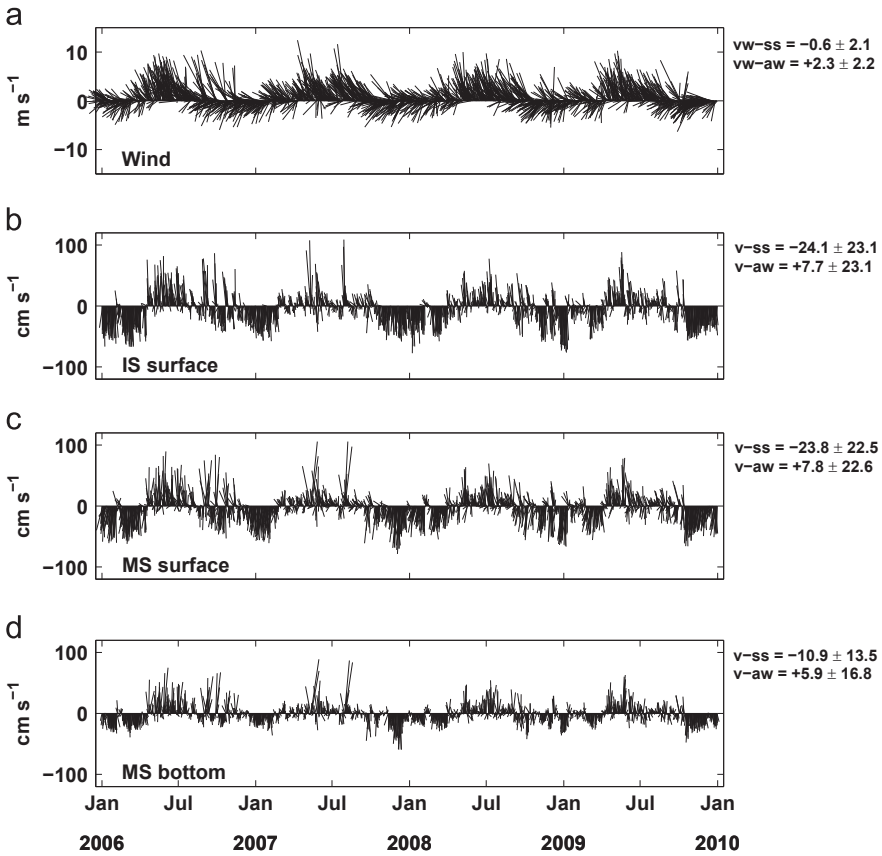

Fig. 4. Modelled time series (2006–2009) of the (b) surface inner-shelf (IS) currents and (c) surface and (d) bottom mid-shelf (MS) currents, coincident with the ACM2 (IS) and ADP (MS) sites presented in Amorim et al. (2011, Fig. 4). (a) Wind time series derived from QuickSCAT for the ADP site. The mean and standard deviations of the wind (vw) and alongshore currents (v) during the spring/summer (ss) and autumn/winter (aw) seasons are presented on the right side of the panels. The vertical axis is aligned parallel to the coastline. See Fig. 3 for the location of the sites.

inner- and mid-shelves of the region of study (~14°, see Fig. 3 for location), which are coincidents with the ACM2 (inner-shelf) and ADP (mid-shelf) sites presented in Amorim et al. (2011). The general aspects of the RCM presented in Fig. 4b–d compare well with Amorim et al. (2011) results (see their Fig. 4 and Table 3), where a marked seasonal cycle is clear. In addition, the wind seasonality derived from a meteorological station and reported by these authors is also clear along the time series (Fig. 4a), presenting prevailing E–NE (E–SE) winds during the spring/summer (autumn/winter) seasons.

Although quantitative comparisons between the observed and modelled results have to be taken with some caution in this case, due to the relatively short time series reported by Amorim et al. (2011), we can use these values to evaluate the mean currents and associated variability. As observed by Amorim et al. (2011), the RCM surface currents over the shelf follow the wind seasonality being southward oriented during the spring/summer seasons with a mean intensity of −24.1 cm s^{-1} (−23.8 cm s^{-1}) at the inner (mid) shelf (Fig. 4b, c). The surface currents show a reversal of the mean flow during the autumn/winter seasons, following a similar pattern of the wind (Fig. 4a), being less intense and more variable due to the more frequency of cold frontal systems passages. The mean intensity and variability of the inner- and mid-shelf surface currents during these seasons are 7.7 ± 23.1 cm s^{-1} and 7.8 ± 22.6 cm s^{-1}, respectively. A seasonal variability is also observed in the barotropic signal. While a current shear is observed along the water column with no change in the orientation of the main flow (Fig. 4c, d), the spring/summer season reveals a more intense stratification along the water column (Amorim et al., 2011, 2012) when compared with the autumn/winter seasons. As a general aspect and although the above dynamics is captured by the RCM, the model results tend to underestimate (overestimate) the mean spring/summer (autumn/winter) currents and are less sensitive to seasonal variations in the variability of the currents. This pattern can be seen in more detail in the current roses for the raw data and model mean results (2006–2009) for the surface currents at the ADP site. The surface currents at the mid-shelf were chosen for comparison since they are more influenced by the atmospheric circulation and WBC, as reported by Amorim et al. (2011, 2012). The results for the autumn season (Fig. 5c, d) are well captured by the model, with currents slightly less intense and to the E–NE direction. The summer currents represented by the model results (Fig. 5b) are less intense and show a tendency to follow the E direction while the raw data (Fig. 5a) show currents that follow the E–SW direction.

For the shelf/slope regions the modelled currents are compared with the geostrophic currents derived from AVISO (2011). Although Fig. 6 is discussed in more details in the next section, our idea here is to focus on the general aspects of the circulation associated with the WBC. For this reason, we decided to use a monthly mean of a given month to represent each season. In this context, the modelled surface currents for the austral spring and summer (Fig. 6a, b) clearly show the southward BC, which is not only in agreement with Soutelino et al. (2011), who argue that north of 20°S the current can be interpreted as the coastal boundary of anticyclones, but also resembles the southward geostrophic currents derived from AVISO south of 12°S and presented in Fig. 7a, b. It is important though, in the comparisons between the modelled and geostrophic currents, to keep in mind that the former are restricted to the slope

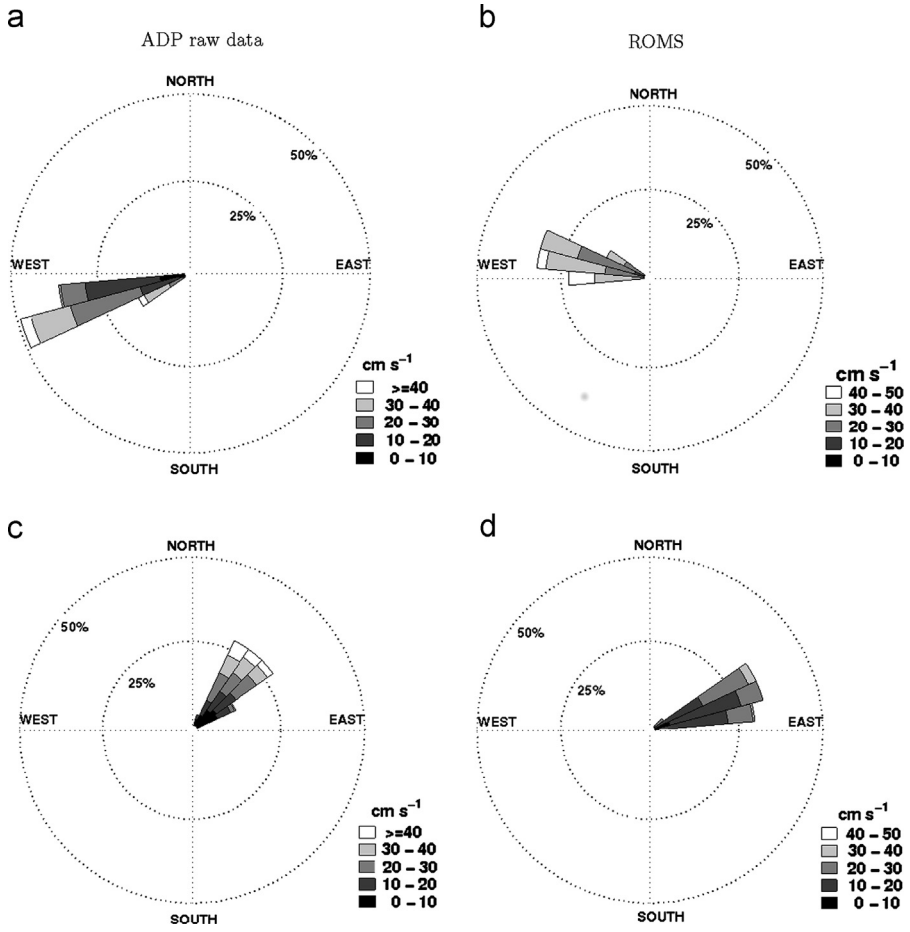

Fig. 5. Current roses for the surface currents at ADP site (see Fig. 4 in Amorim et al., 2011) and model results (2006–2009) at the same site, for the months representative of (a, b) summer and (c, d) autumn seasons.

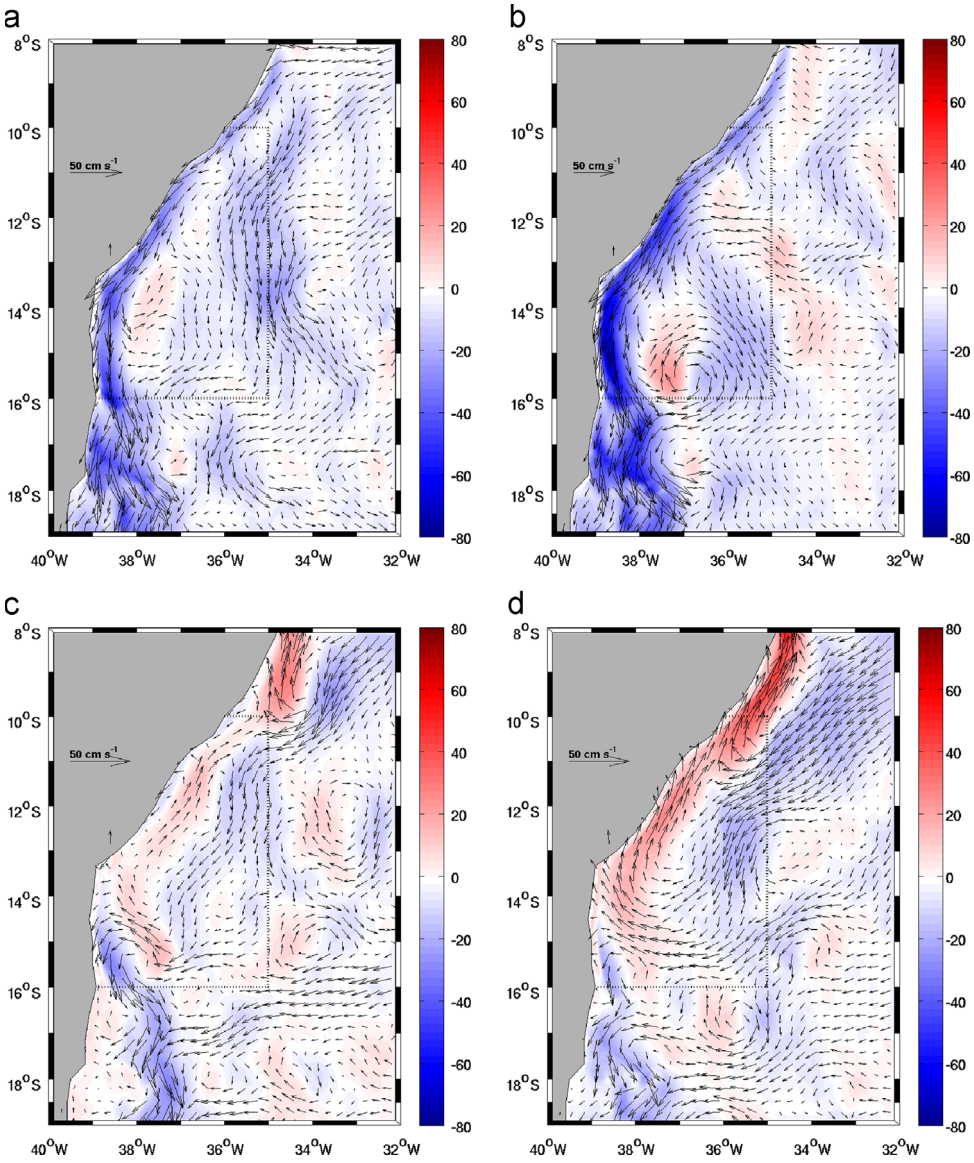

Fig. 6. Monthly mean (2006–2009) horizontal surface currents (vectors) derived from the RCM for the months of: (a) October, (b) January, (c) April and (d) July. The shaded area represents the intensity (cm s^{-1}) of the meridional velocity component, where positive values are equatorward. The area inside the dotted lines represents the region of study.

regions deeper than 200 m, due to the altimeter limitation. The reversion of the WBC during the autumn and winter seasons, where the modelled northward NBC/NBUC is present north of 15°S (Fig. 6c, d), is also in agreement with the geostrophic currents shown in Fig. 7c, d. In addition, and with no sign of seasonality, both modelled and geostrophic currents show a continuous southward BC south of 17°S.

Regarding the transport associated to the WBC, Fig. 8 presents the mean transport in the slope region at 11°S, and for the first ~1200 m of the water column, which includes the TW, SACW and AAIW (Antartic Intermediate Water) water masses. The results reflect the dominance of the NBC/NBUC flow at this latitude and also the influence of the north–south displacement of the SEC bifurcation between seasons (Fig. 8). During March (Fig. 8a), the mean northward transport is +19.0 Sv and increases to +28.2 Sv during August (Fig. 8a), when the SEC bifurcation is at its southernmost position (~17°S in July) and the NBUC flow increases (Rodrigues et al., 2007). The southward transport shows a slightly increase between these months, from −1.4 Sv to −1.98 Sv. These results are also in good agreement with those presented by Schott et al. (2005) (see their Fig. 6b), based on observed ADCP/LADCP profiles.

The model was also able to capture the variability in the termohaline structure. The comparison between temperature and salinity mean profiles from the model results with 835 ARGO floats (Fig. 9) found into the region of study between 2006 and 2009 shows that the model was capable to represent the interannual variability in temperature and salinity, with mean values inside the standard deviation limits. The salinity contraction found below 1200 m depth was also in good agreement with the ARGO profiles. The only exception was the mean salinity of the modelled mixed layer, which while inside the ARGO standard deviation limits, is lower than the mean observed values. (blue shaded in Fig. 9).

4. Results

The results presented in the following sections, when not specified, have their focus on the region between the zonal range

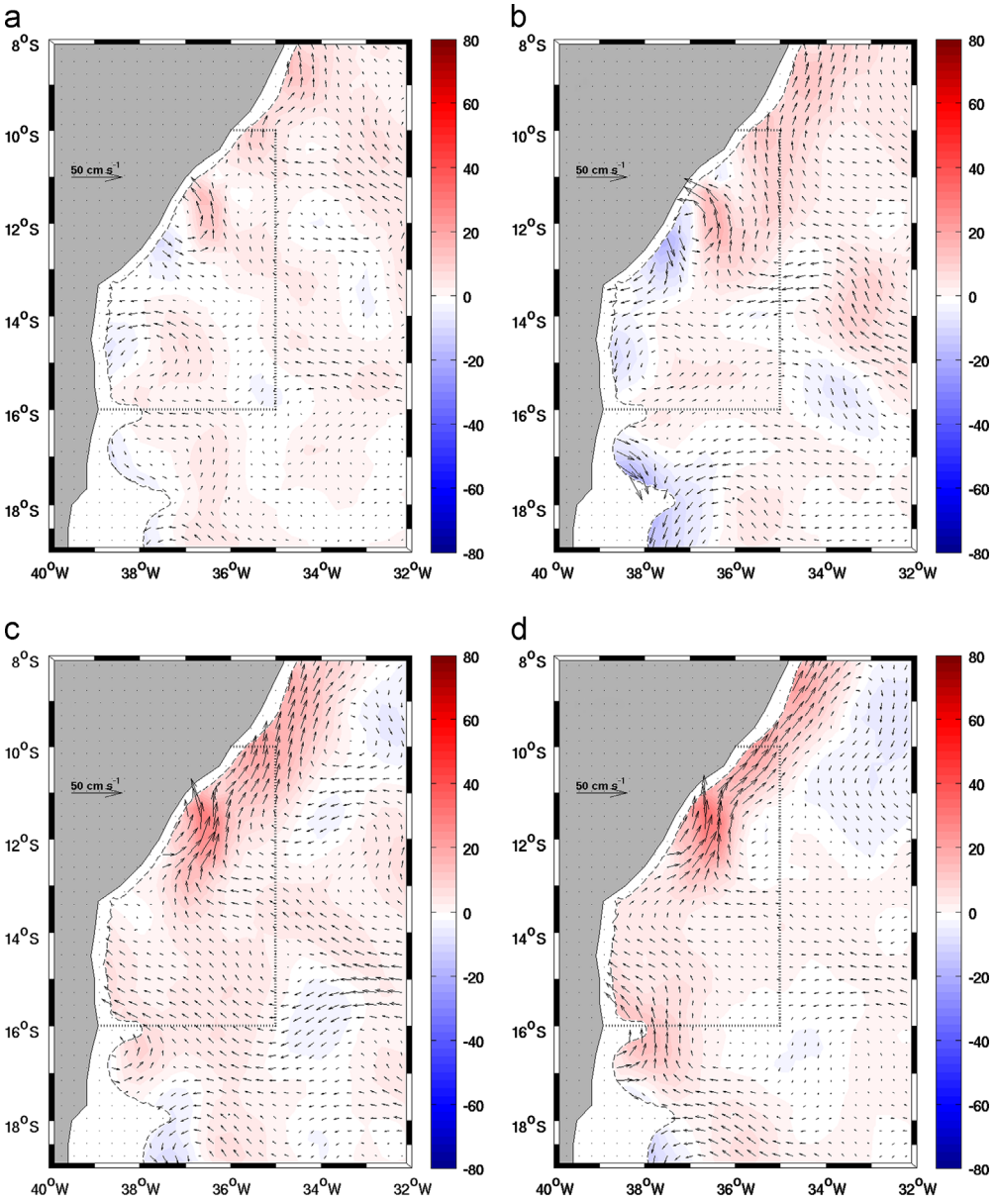

Fig. 7. Monthly mean (2006–2009) geostrophic currents (vectors) derived from AVISO (2011) for the months of: (a) October, (b) January, (c) April an (d) July. The shaded area represents the intensity (cm s^{-1}) of the meridional velocity component, where positive values are equatorward. The area inside the dotted lines represents the region of study. Regions where the depth is shallower than 200 m are not presented.

from 10°S to 16°S and the meridional range from 35°W to the coast (Fig. 3). The analysis includes the tidal circulation, the seasonality of the shelf/slope circulation and a discussion of the forcing mechanisms related to the circulation. The seasonal analysis is related to the four austral seasons: Spring (October, November and December), Summer (January, February, March), Autumn (April, May, June) and Winter (July, August, September).

4.1. The tidal circulation

According to Table 2, the tides at the region of study are dominated by the semi-diurnal M_2 component, followed by the semi-diurnal S_2 component which presents an amplitude almost 50% of the former. This behaviour gives a semi-diurnal tidal pattern to the region of study.

The horizontal distribution of the amplitudes and phases for the main semi-diurnal and diurnal tidal components (M_2, S_2, O_1 and K_1) over the domain (Fig. 10) based on the harmonic analysis (Pawlowicz et al., 2002) of the RCM sea surface height time series (2006–2009) shows that the tidal wave propagates northward, following the Kelvin wave dynamics, with the highest amplitudes observed on the northern portion of the domain. Although the coastal tidal amplitudes were not too different from those at the deep ocean, which could be related to the narrow width of the shelf, the amplitude values show a tendency to increase toward the coast and the phase lines are aligned perpendicular to the coastline. The highest amplitude is observed for the semi-diurnal M_2 component (Fig. 10a), with values around 70 cm, followed by the semi-diurnal S_2 component (Fig. 10b), which presents amplitudes almost half of the M_2 component. The main diurnal components present a similar pattern, but, while the K_1 component presents the highest value of ~5 cm at the northern region (Fig. 10d), the O_1 component presents the highest value at the coastal region and around 7 cm (Fig. 10c). When the tidal amplitudes and phases derived from the RCM are compared with those provided by the TPXO model (not shown), one can clearly detect that the better

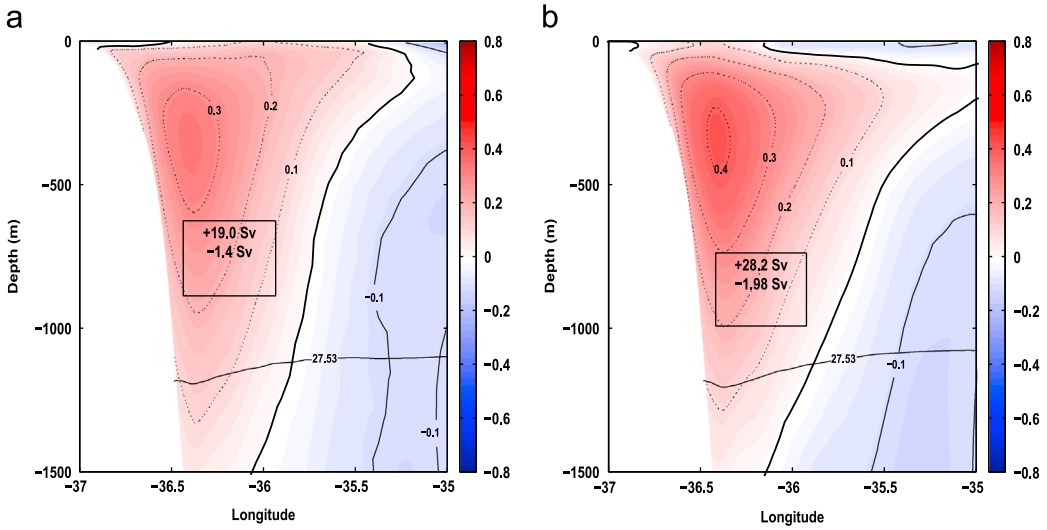

Fig. 8. Mean vertical section (2006–2009) of the alongshore velocity (m s^{-1}), positive (red shade) northwards, at 11°S for the months of (a) March and (b) August. The dashed line indicate the lower isopicnal limit of the AAIW water (27.53 kg m^{-3}). (For interpretation of the references to colour in this figure caption, the reader is referred to the web version of this article.)

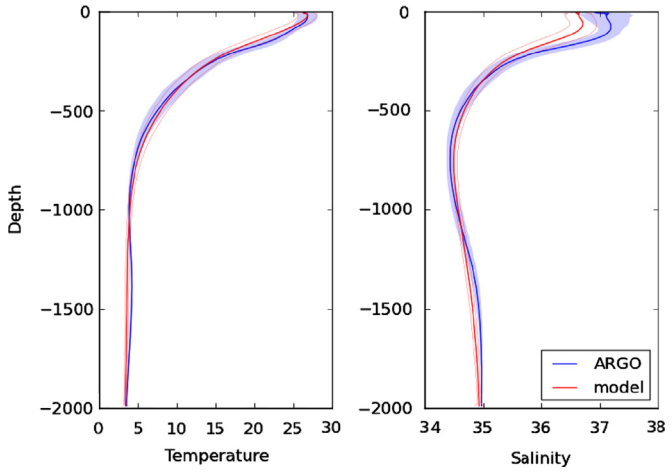

Fig. 9. Mean vertical profiles of Temperature and Salinity from the model results (red lines) and from 835 ARGO floats (blue lines) found in the region of study between 2006 and 2009. The light red lines and blue shades represent, respectively, the model and ARGO standard deviations from the mean value. (For interpretation of the references to colour in this figure caption, the reader is referred to the web version of this article.)

resolved topography of the RCM gives rise to more complex patterns of the amplitudes and phases distribution over the domain.

The barotropic tidal ellipses for the main tidal components, calculated with the same methodology adopted for the tidal amplitudes/phases, but for the barotropic current time series, are presented in Fig. 11. The blue (red) ellipses have a counterclockwise (clockwise) rotation. The ellipses for the semi-diurnal M_2 and S_2 components (Fig. 11a, b) show a clockwise rotation over the oceanic region and an alongshore orientation, following the Kelvin waves dynamics, with a mean intensity of 1.5 cm s^{-1} and 0.5 cm s^{-1}, respectively. However, at the southern of the domain, these ellipses show a tendency to be aligned 45° to the coast and present a higher eccentricity. This behaviour could be related to the AbB topography on the southern portion of the domain which implies an alignment parallel to the local isobaths (see Fig. 5 of Pereira et al. (2005)). Over the shelf/slope region, these ellipses show preferentially a counterclockwise rotation, an alignment perpendicular to the coastline, less eccentricity and a velocity intensification with a mean value of 4 cm s^{-1} (1.5 cm s^{-1}) and a maximum value of 120 cm s^{-1} (38 cm s^{-1}), aligned at the SSA channel (not shown), for the M_2 (S_2) component. This behaviour could be a response to the bathymetric irregularities at the coastal region which have great influence on the velocity field adjustment being responsible for the tidal currents amplification and reversal of the ellipses rotation direction, as reported by Pereira et al. (2005) for the AbB region.

The ellipses for the main diurnal components (Fig. 11c, d) are mostly aligned parallel to the coastline over the entire domain, presenting great eccentricity and a tendency for clockwise rotation, with almost no change over the shelf/slope region. However, it presents a relative increase toward the coast with mean intensity of 0.5 cm s^{-1} (0.4 cm s^{-1}) and major intensity of 10 cm s^{-1} (8 cm s^{-1}) aligned at the SSA channel (not shown) for the O_1 (S_1) component.

4.2. The shelf/slope seasonal circulation

4.2.1. Horizontal circulation

Since we are interested on the hydrodynamics over the shelf/slope region, the seasonal (2006–2009) horizontal circulation is evaluated over the whole model domain for the first 1000 m of the water column, which includes the main water masses that occupy the study region: the warm TW, the SACW and the upper part of the Antarctic Intermediate Water (AAIW). As presented in Section 2, the circulation dynamics at the region of study for the first 400 m is highly influenced by the annual meridional displacement of the ITCZ, presenting distinct scenarios between spring/summer and autumn/winter seasons. As a response, the surface circulation is mainly affected by the large scale seasonality of the trade winds and the circulation at the 100/150 m depth is highly influenced by the associated seasonal excursion cycle of the SEC bifurcation. Hence, in order to capture this cycle, the horizontal circulation at these levels is investigated for the following months: October (austral spring), January (austral summer), April (austral autumn) and July (austral winter). For the 300 m and 800 m levels, the circulation is investigated based on the annual mean only.

During the spring/summer seasons the surface currents (Fig. 6a, b) are under the influence of E–NE winds south of ~12°S (Fig. 2a, b), driving shelf/slope currents with a mean southward flow and a marked intensification poleward. A maximum value of −0.75 m s^{-1} is reached during January and between 14°S and 16°S. During this season, two mesoscale features are observed, an

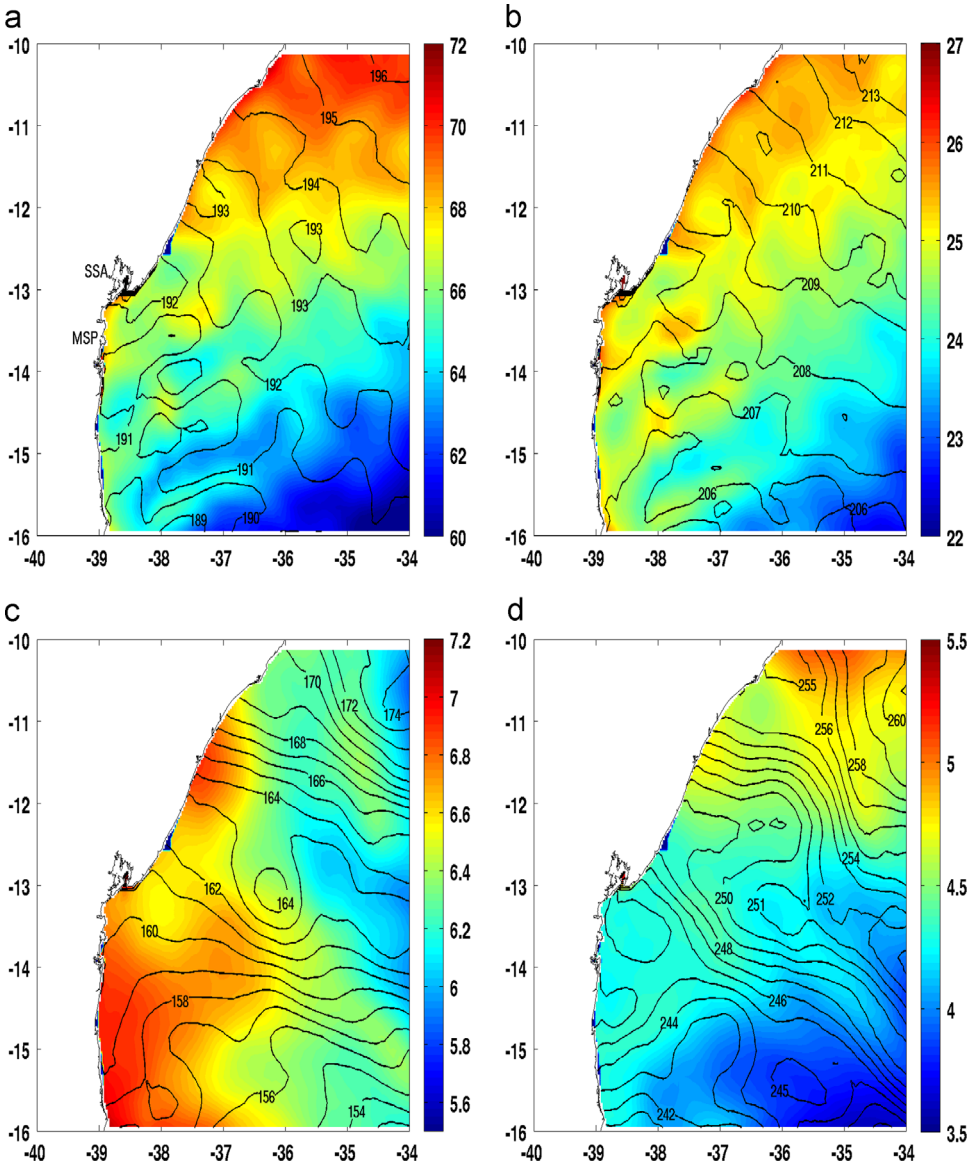

Fig. 10. Amplitudes (cm) and Greenwich phases (degrees) of the main semi-diurnal (a) M_2 and (b) S_2 and diurnal (c) O_1 and (d) K_1 tidal components calculated from the RCM sea surface height. The SSA and MSP sites are presented at the M_2 component panel.

intense cyclonic eddy north of the RCB (~16°S) and centred at 37°W, and an anticyclonic eddy southward. According to Rezende et al. (2011), the irregular topography between the RCB and AbB (~18°S) constrains and alters the flow, inducing variabilities on the physical, chemical and biological properties over the shelf and adjacent regions. Irregularities of the flow are also observed over RCB and AbB regions during October (Fig. 6a), where a maximum intensity of 0.52 m s^{-1} occurs.

Following the seasonal changes of the winds, during the autumn/winter seasons the surface shelf/slope currents (Fig. 6c, d) north of 16°S show a complete reversal of the mean flow as a response of the preferential E–SE winds (Fig. 2c, d), presenting a mean northward flow and a marked intensification equatorward. During the autumn season, the coastal border of a cyclonic eddy north of 10°S intensifies the northward flow over the shelf (Fig. 6c). For the same season, a sequence of anticyclonic eddies over the AbB region generates a less intense and southward flow at the inner- and mid-shelves. During the winter season, a cyclonic pattern circulation can be observed between 11°S and 16°S latitudes (Fig. 6d), which limits the beginning of a northward flow. South of this region, the presence of an anticyclonic circulation over the RCB imposes a southward flow over the shelf.

At the 100 m depth, the sub-surface circulation is dominated by the seasonal flows of the southward BC and the northward NBUC, following the seasonal meridional excursion of the SEC bifurcation. As a response, during October (Fig. 12a), the northward NBUC flow starts at ~15°S and the coastal borders of three anticyclones confined between the RCB and AbB regions and centred at about 15°S, 17°S and 19°S could represent the southward BC flow. This pattern was reported by Soutelino et al. (2011), based on non-divergent velocities derived from ADCP data. During January (Fig. 12b), the origin of the northward NBUC is observed at ~13°S with an organized flow from ~12°S. South of this latitude, the remaining effect of the cyclonic eddy observed at the surface (Fig. 6b) added to coastal anticyclones originates a complex circulation pattern. The SEC bifurcation keeps migrating southward during April, when the beginning of the northward NBUC flow is observed at ~16°S (Fig. 12c) and its southernmost position occurs in July, when the origin of the northward NBUC flow is observed at ~17°S (Fig. 12d). The presence of anticyclonic eddies at the RCB and AbB regions imposes a weak southward flow (Fig. 12c, d), probably associated with the southward BC. In general, a considerable equatorward intensification

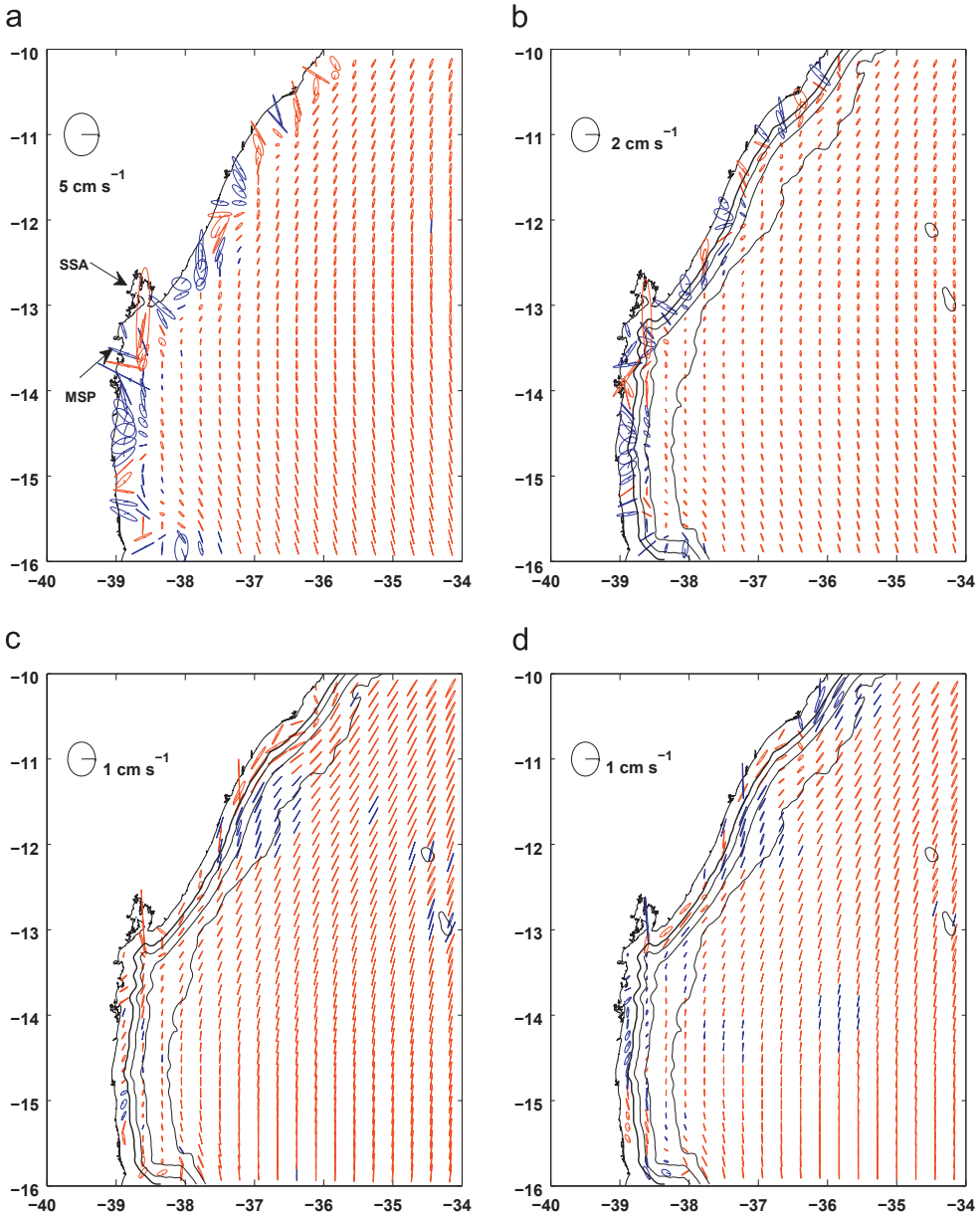

Fig. 11. Barotropic tidal ellipses of the main semi-diurnal (a) M_2 and (b) S_2 and diurnal (c) O_1 e (d) K_1 tidal components calculated from the RCM barotropic currents. Blue (red) ellipses are counterclockwise (clockwise). The radial line inside the ellipses gives the Greenwich phase. The ellipses scale represents a circular ellipse with semi-axis of 5 cm s^{-1} (2 cm s^{-1}) for the semi-diurnal M_2 (S_2) tidal component, and a semi-axis of 1 cm s^{-1} for the diurnal O_1 and K_1 tidal components. The SSA and MSP sites are presented at the M_2 component panel. (For interpretation of the references to colour in this figure caption, the reader is referred to the web version of this article.)

of the northward NBUC flow is also observed along the whole seasonal cycle.

A meridional displacement of the SEC bifurcation also occurs along the water column, reaching ~22°S between 200 m and 400 m (Stramma and England, 1999; Silveira et al., 2000; Cirano et al., 2006). As a result, at 300 m depth the SACW is transported northward by the NBUC flow over the whole domain with a strong intensification toward the equator (Fig. 13a). A similar pattern occurs for the AAIW, where at the depth of 800 m a northward flow is present over the slope (Fig. 13b). According to Stramma and England (1999), the bifurcation at this level occurs at about 25°S.

4.2.2. Vertical circulation

Aiming to investigate the vertical structure of the circulation on the EBS and its spacial and seasonal variability, three radials perpendicular to the coastline were defined as shown in Fig. 3. In order to capture the influence of the seasonal transition of the BC and NBC/NBUC flow domain (Rezende et al., 2011), a central radial was defined at 14°S (hereafter R14). A radial north of this latitude was established at 10°S (hereafter R10) with the purpose of capture the influence of the more frequent episodes of the NBC/NBUC flow dominance (Silveira et al., 1994; Schott et al., 2002). Finally, a southernmost radial was established at 16°S (hereafter R16), which is more dominated by the BC flow and also presents more mesoscale activity associated to the constrain of the flow over the RCB and AbB regions (Rezende et al., 2011; Soutelino et al., 2011). Since one of the goals of this study is to investigate the seasonal variability of the circulation over the shelf/slope and its interaction with the WBC, the vertical structure was evaluated following the changes between spring and winter seasons. In addition, the eastern limit of each radial was defined in order to incorporate the core of the WBC and the associated water masses along the slope region (TW and SACW), whose dynamics can affect

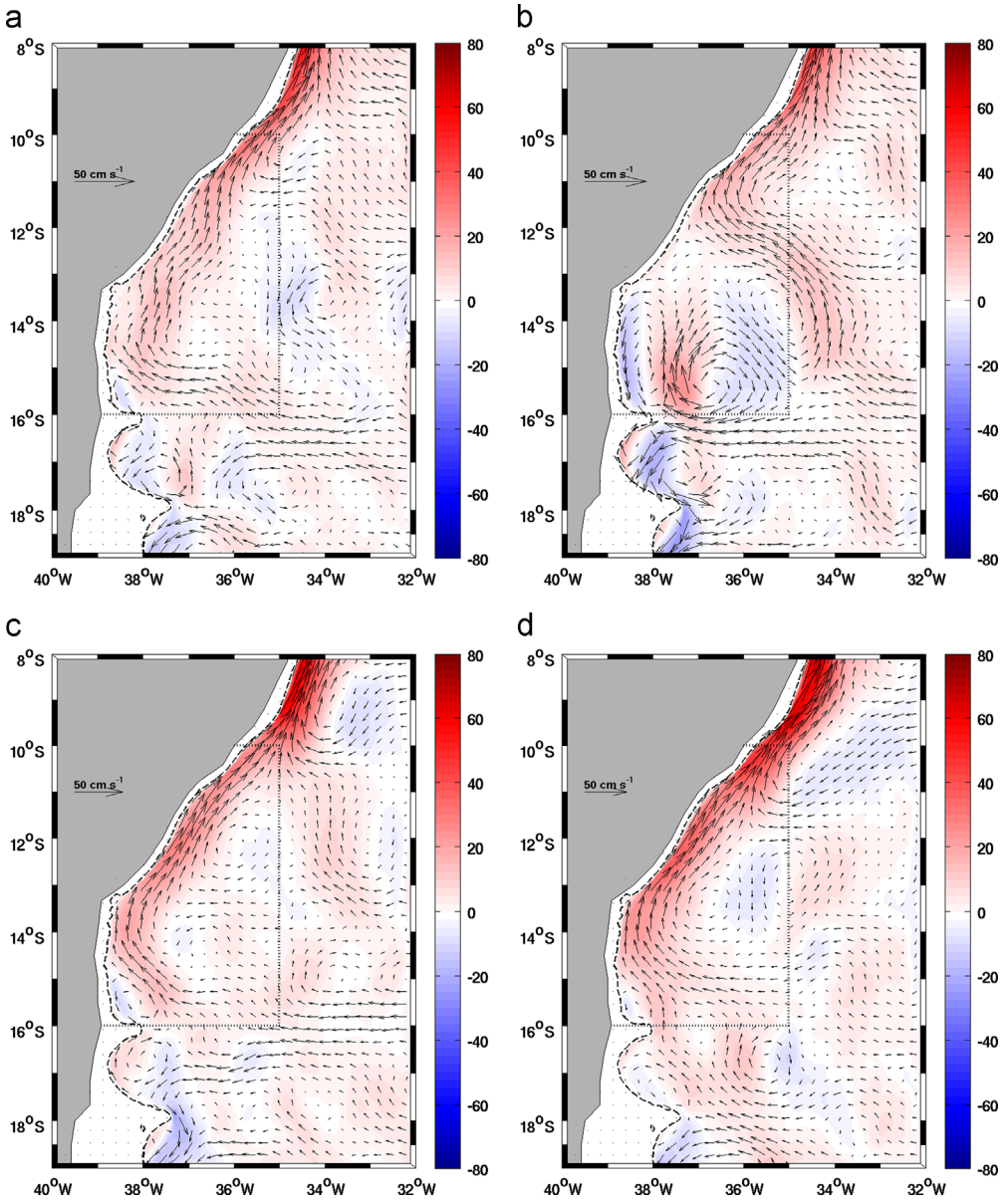

Fig. 12. Monthly mean (2006–2009) horizontal currents at the depth of 100 m (vectors) derived from the RCM for the months of: (a) October, (b) January, (c) April and (d) July. The shaded area represents the intensity (cm s^{-1}) of the meridional velocity component, where positive values are equatorward. The area inside the dotted lines represents the region of study.

the mean flow over the shelf. Thus, R10 was delimited between the coast and 35°W, R14 between the coast and 38°W and R16 between the coast and 37°W. The wider of R16 is due to the RCB topography.

During October, when the SEC bifurcation is close to its northernmost position and associated with the local wind pattern, a southward flow is observed in the upper 50 m in the northern radial (R10) , which occupies the whole shelf width (R10, Fig. 14a). This flow transports a small portion of TW, with a maximum intensity of −0.21 m s^{-1}. Underneath (~50–150 m), the major portion of TW is carried northwards by the NBC/NBUC flow, with a mean intensity of +0.20 m s^{-1}. Between ~150 and 400 m depth, the SACW is carried by the northward NBUC, reaching a maximum intensity of +0.70 m s^{-1} at the core of the current. During January (Fig. 14d), the surface southward flow not only increases but broadens, transporting the TW with a maximum intensity of −0.35 m s^{-1} over the slope. Between 50 and 150 m the TW is carried northward by the NBUC flow, with a maximum intensity of +0.30 m s^{-1}. Underneath, the northward NBUC flow slightly increases and transports the SACW with a maximum intensity of +0.42 m s^{-1}. Following the southward SEC bifurcation excursion during the autumn/winter seasons, during April (Fig. 14g) the major portion of TW is carried northwards by the NBC/NBUC, with an intensity of up to +0.35 m s^{-1}, while a weak southwards flow is confined over the shelf. At the sub-surface level, the NBUC flow increases carrying the SACW with a maximum intensity of +0.42 m s^{-1}. During July (Fig. 14j), the SEC bifurcation reaches its southernmost position and the NBC/NBUC system occupies the whole shelf/slope region, carrying the TW/SACW northwards with an intensity up to +0.63 m s^{-1} at the core of the current.

At R14, a similar seasonal pattern to that at R10 is observed, with a clear intensification (weakening) of the BC (NBC/NBUC) flow (Fig. 14b, e, h, k). During October (Fig. 14b), the BC flow presents a well organized southward flow at the first 100 m depth and occupies the entire shelf/slope region, with a maximum intensity of −0.34 m s^{-1}. At the sub-surface level, the SACW is

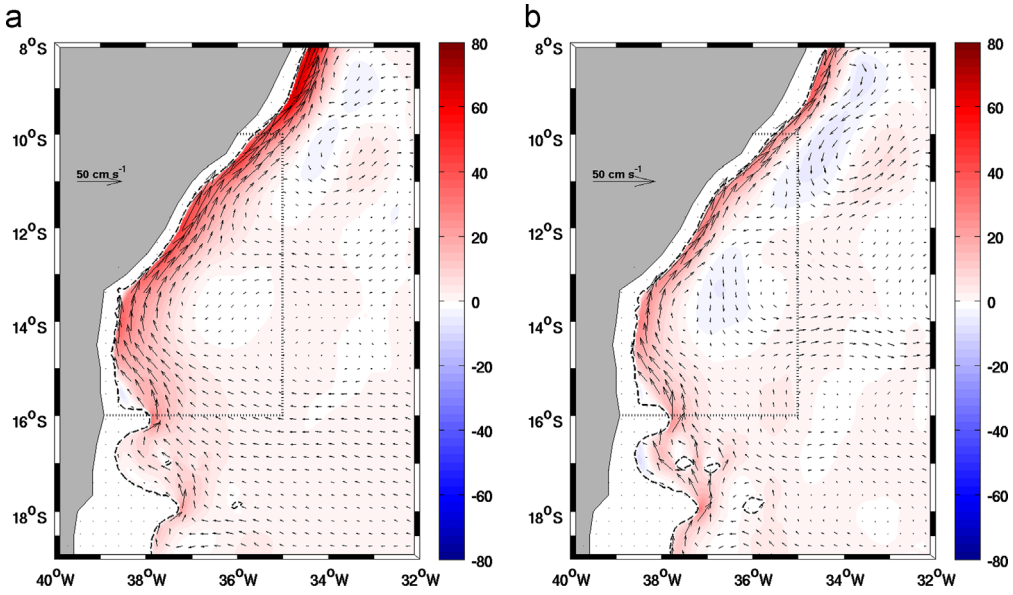

Fig. 13. Monthly mean (2006–2009) horizontal currents at the depth of (a) 300 m and (b) 800 m (vectors) derived from the RCM. The shaded area represents the intensity (cm s^{-1}) of the meridional velocity component, where positive values are equatorward. The area inside the dotted lines represents the region of study.

transported by the NBUC flow with a mean speed of +0.24 m s^{-1}. Below 100 m depth, a small portion of the SACW is upwelled, leading to an increase of the thickness of this water mass in comparison to what is observed at R10 radial for the same month. During January (Fig. 14e), the BC flow increases and deepens, carrying the major part of TW southwards, with a maximum intensity of −0.62 m s^{-1} over the slope. Below 150 m depth, the northward NBUC flow decreases and reach its minimum value during the whole year. In addition and in analogy to what was observed during October, a slight upwelling of the SACW over the slope was observed. During April–July (Fig. 14h, k), and following the decrease of the BC flow, the TW is mainly carried northwards, with a mean velocity of +0.18 m s^{-1} during July. During this same month, the maximum core speed of the NBUC was observed, with a flow of +0.42 m s^{-1} over the slope.

At R16 (Fig. 14c, f, i, l), a permanent surface southward flow over the shelf/slope region and a marked mesoscale activity (see Figs. 6 and 12) is captured. The later is probably ascribed to the flow constrain due to the RCB topography, which alters significantly the circulation pattern between seasons. During October (Fig. 14c), the BC presents itself as a well organized surface flow occupying the whole shelf/shelf-break region and carrying the TW preferentially southwards, with a maximum intensity of −0.61 m s^{-1} over the shelf. Underneath, the SACW is transported northwards by the NBUC, presenting a core of +0.35 m s^{-1} over the slope. During January (Fig. 14f), the southward BC is now confined to the shelf region, with a maximum flow of −0.43 m s^{-1}. At the offshore region, the coastal border of the cyclonic eddy observed during this month (Figs. 6b and 12b) imposes a northward flow between the surface and the depth of 150 m, which transports the TW equatorwards over the slope. During April (Fig. 14i), the BC intensity decreases and flows over the shelf/shelf-break region with a maximum intensity of −0.12 m s^{-1}. The surface recirculation observed during this month (Fig. 6c) generates a weak northward flow at the inner-shelf. At the sub-surface level, a weakening of NBUC is observed, presenting a core with intensity of +0.21 m s^{-1}. During July (Fig. 14l), the anticyclonic eddies that occur at the RCB region (Figs. 6d and 12d) constrain a southward flow over the shelf, with a maximum intensity of −0.20 m s^{-1}, and, as a result, part of the TW is carried southwards over the shelf and part is carried northwards over the shelf-break/slope region. The NBUC shows a well organized core over the slope, carrying the SACW northwards with a mean intensity of +0.25 m s^{-1}.

4.2.3. Associated transport

The monthly mean transports associated to the TW and SACW layers, between the limits of the three radials described above, are presented in Fig. 15. The results show that the southward flow at the surface layer increases polewards from an annual mean value of −0.48 Sv at R10 (Fig. 15a, solid line) to −1.66 Sv at R16 (Fig. 15c, solid line). As a response, the annual net transport at R10 (+1.93 Sv) is northward oriented, while at R14 and R16 radials is southward oriented. This pattern may suggest that the northward flow is dominant at radial R10, while at radials R14 and R16 an alternate dominance between the northward/southward flows occurs. At the sub-surface level and for the SACW layer (Fig. 15b, d, f), the transports over the slope are clearly dominated by the northward flow, with a net increment of +3.69 Sv between R16 (+4.15 Sv) and R10 (+7.84 Sv). Taking into account that the results described are based on the TW and SACW layers and delimited by the radials presented in Fig. 14, the results are in good agreement with Rodrigues et al. (2007), Silva et al. (2009) and Rezende et al. (2011).

Evaluating the annual cycle, and for the TW layer, at R10 the northward flow is the dominant pattern along the year, with a marked seasonal cycle and a maximum transport of 3.04 Sv in May. At R14 and R16 there is an alternate dominance between the southward/northward flows at TW layer, with the dominance of the southward (northward) flow between October and February (March and September) months at R14. At the SACW layer, there is a clear dominance of the northward flow over the year for the three radials, although a small southward transport occurs.

4.3. The forcing mechanisms for the shelf/slope circulation

To evaluate the time and space variability of the circulation at EBS, four stations (red dots in Fig. 3) were distributed at each of the R10, R14 and R16 radials, being located at the inner-shelf, mid-shelf, shelf-break/slope and at the oceanic region, respectively. The offshore stations were chosen to be aligned with the

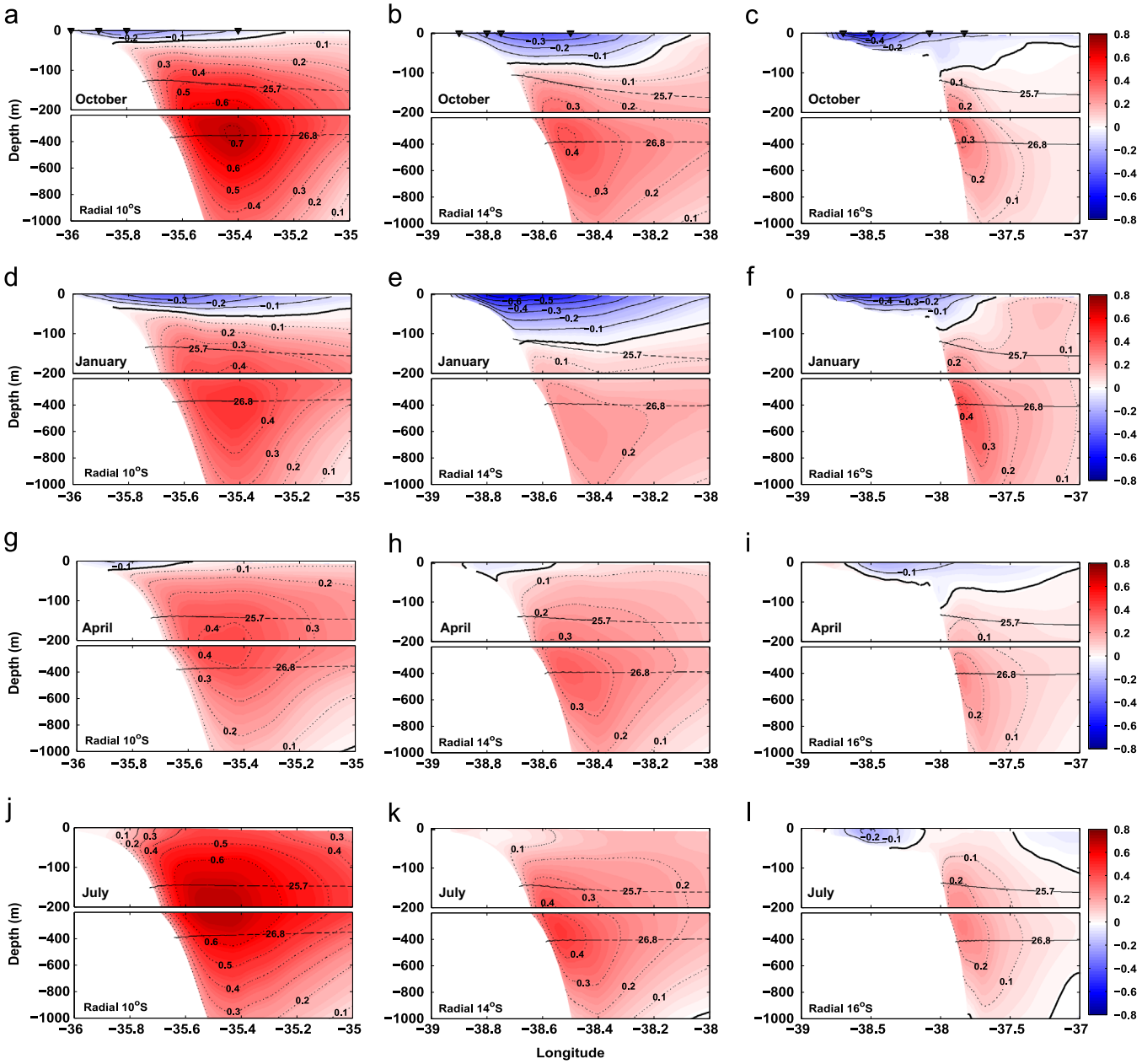

Fig. 14. Mean vertical sections (2006–2009) of the alongshore velocity (m s^{-1}), positive (red shade) northwards, at R10 (left), R14 (middle) and R16 (right) radials for the months (top to bottom) of: October, January, April and July. The dashed lines indicate the isopicnal limits between the TW ($\sigma_\theta < 25.7$ kg m^{-3}) and SACW (25.7 kg m^{-3} $< \sigma_\theta < 26.8$ kg m^{-3}). The location of the stations adopted for the time series analysis is indicated at the October figures. See Fig. 3 for the geographical position of both radials and stations. (For interpretation of the references to colour in this figure caption, the reader is referred to the web version of this article.)

mean core of the SACW at each radial, based on the seasonal vertical sections of the alongshore velocity presented in Fig. 14.

The analysis is made based on the sub-inertial time-series (2006–2009) of the alongshore (v) and cross-shore (u) components of the velocity at both surface and bottom. The sub-inertial time-series of the alongshore component of the wind, derived from QuickSCAT for a point close to the stations at each radial, are also used to investigate the response of current to the meteorological forcing, based on the lagged cross-correlation functions (e.g. Orfanidis, 1998) between them.

Aiming to understand how the WBC dynamics influence the circulation within the shelf, we also investigated the lagged cross-correlation functions between the alongshore component of the depth-integrated current at the inner-shelf, mid-shelf and shelf-break/slope regions with that at the adjacent oceanic region. For the oceanic region only, the alongshore component of the velocity was depth integrated from the surface to the local depth of the nearby shelf-break/slope station. With this approach, we believe that we can evaluate the seasonal variability of the WBC that flows and moves vertically at the slope region and eventually occupies the shelf and influences its dynamics, as can be observed during July (Fig. 14j–l).

The sub-inertial time-series were obtained with the digital filter proposed by Walters and Heston (1982), with a cut-off period of 72 h, which covers the inertial period between the 10°S (~69 h) and 16°S (~ 43 h) latitudes. In order to obtain the alongshore component of the velocity, for the R10 radial (Fig. 3) only, a rotation of 45° to the true north was applied to the currents and winds, in accordance with the orientation of the local isobaths.

Since the ocean variability in the study region is mainly driven by the seasonal changes in the large scale atmospheric circulation,

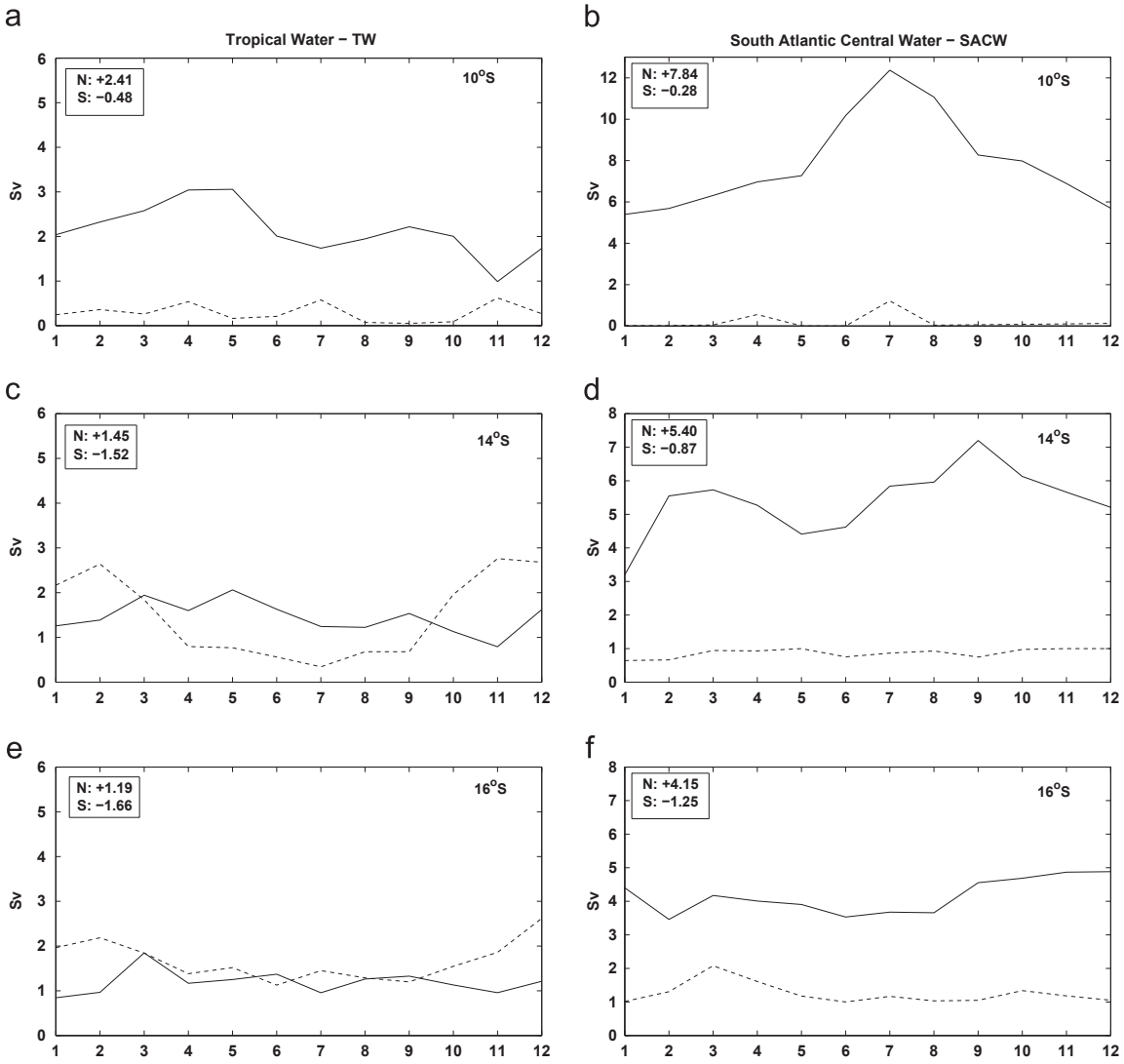

Fig. 15. Annual cycle of the monthly mean (2006–2009) transport (Sv) estimates along the (a, b) R10, (c, d) R14 and (e, f) R16 radials for the TW (left) and SACW (right) layers, limited by the isopicnals of $\sigma_\theta < 25.7$ kg m^{-3} and 25.7 kg m$^{-3} < \sigma_\theta < 26.8$ kg m^{-3}, respectively. Positive (negative) northward (southward) transports are represented by the solid (dashed) lines. The annual mean transports for each direction are indicated inside the boxes. 1 Sv = 10^6 m^3 s^{-1}. See Fig. 3 for the location of the radials.

which influences the large scale oceanic circulation, we adopted two different periods to analyse the currents variability, the spring/summer and autumn/winter seasons. This approach was also used by Amorim et al. (2011, 2012) and has the purpose of highlighting the major variations among the different seasons, grouped in two different scenarios.

4.3.1. Spring/summer scenario

The alongshore surface circulation at radial R10 (Fig. 16b–e) follows the preferential southward wind forcing (Fig. 16a) and the alongshore bottom currents show the influence of the currents at the slope region, which are in opposite direction with a mean northward flow, with the exception of inner-shelf (Fig. 16b). The surface alongshore currents decrease toward offshore with the mean intensity varying from −33.8 cm s^{-1} at mid-shelf to −16.5 cm s^{-1} at the oceanic region, where the alongshore sub-surface (depth of 150 m) currents are more intense (+33.5 cm s^{-1}) than those along the shelf, due to the presence of the northward NBUC flow. As a response to this pattern, the correlation (γ^2) between the alongshore depth-averaged currents at the oceanic region with those over the shelf (Table 3) is higher for the shelf-break region ($\gamma^2 > 0.7$) with almost no lag and decreases toward the coast (with $\gamma^2 = 0.47$ at the inner-shelf). On the other hand, the correlation between the alongshore surface currents with the alongshore wind component (Table 4) is higher at the inner-shelf ($\gamma^2 > 0.62$), decreasing toward the oceanic region ($\gamma^2 = 0.3$). Also, the correlation pattern in the cross-shore direction at the inner- and mid-shelves reflects the effect of the Ekman transport, where the surface (bottom) currents are out-of-phase (in-phase) with the alongshore wind component (Table 4).

At radial R14, the influence of the dynamics associated with the WBC and meteorological forcing is more expressive (Fig. 17b–e), with the forcing mechanisms varying along the shelf according to the seasons. During the spring/summer seasons, the mean alongshore flow over the shelf and slope region is well defined, being southward oriented along depth with a mean surface currents increasing from −11.2 cm s^{-1} at the inner-shelf to −47.3 cm s^{-1} at the shelf-break. Apart from the inner-shelf, the flow along the water column is associated with a strong vertical shear. At the inner-shelf, the alongshore currents (Fig. 17b) present a strong barotropic signal with a high correlation along depth with the alongshore wind forcing ($\gamma^2 > 0.73$, Table 4). The low correlation and negative phase relationship between the inner-shelf depth-averaged currents with those at the oceanic region (Table 3) is a

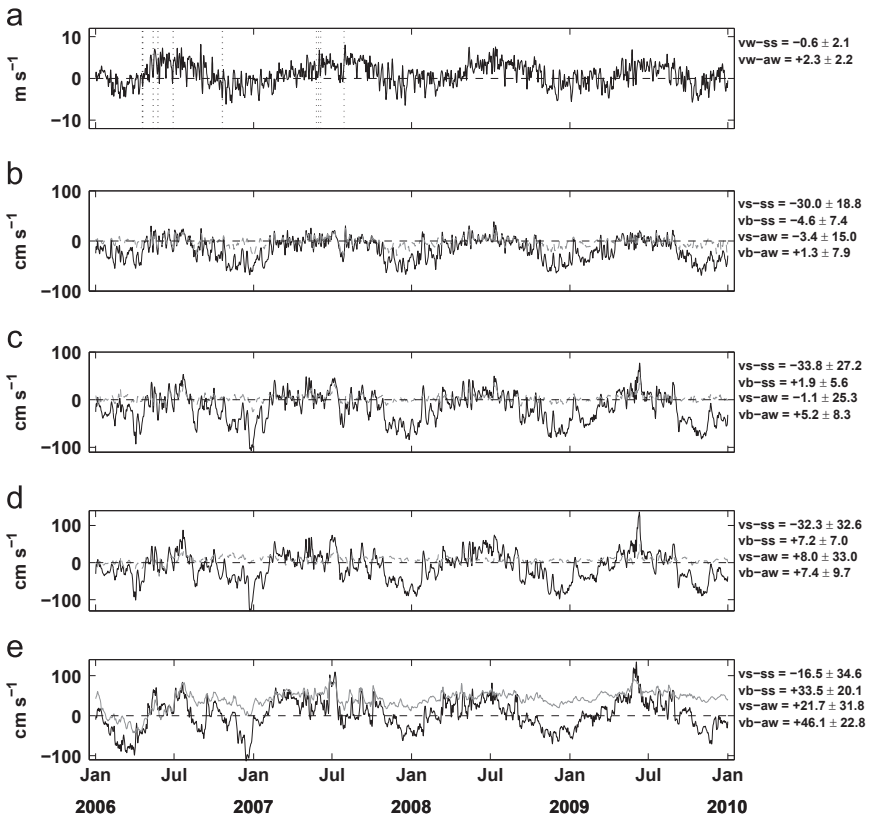

Fig. 16. Sub-inertial time-series (2006–2009) of the alongshore surface (black lines) and bottom/150 m (gray lines) currents at the (b) inner-shelf (IS), (c) mid-shelf (MS), (d) shelf-break (SB) and (e) oceanic region (OR) at radial R10. (a) The sub-inertial alongshore wind time-series derived from QuickSCAT for a point located close to the current time-series. The dotted vertical lines represent the cold-front passages (Inpe, 2011). The associated mean and standard deviation of the alongshore components of the wind (vw), and surface (vs) and bottom (vb) currents during the spring/summer (ss) and autumn/winter (aw) seasons are presented on the right side of the panels. The vertical axis is oriented in the NE/SW direction. See Figs. 3 and 14a for the geographic location of the stations.

suggestion that the wind is the main forcing mechanism at this region. In addition, the high positive correlation ($\gamma^2 > 0.73$) along depth between inner-shelf cross-shore currents and alongshore wind indicates that at this region the surface and bottom Ekman layers interact. At mid-shelf and shelf-break region (Fig. 17c, d), alongshore depth-averaged currents increase their correlation with those at the slope region (Table 3), reaching values above 0.5. The surface alongshore currents at mid-shelf also present a significant coherence ($\gamma^2 = 0.52$) with the alongshore wind forcing (Table 4), but in the cross-shore direction only the bottom currents present a significant coherence ($\gamma^2 = 0.68$) with this forcing.

At the shelf-break and oceanic regions of radial R14 (Fig. 17d, e), the alongshore currents reflect the influence of the dynamics associated with the WBC. At both regions, the bottom currents present low mean intensity and high variability, which could be associated with the presence of the opposing BC and NBUC flows at the shelf-break/slope (Fig. 14b, e) that can eventually interact. This pattern influences the currents along depth, where a higher vertical shear is observed when compared to the currents at the inner- and mid-shelves.

At radial R16 a mean surface southward flow is observed during all seasons (Figs. 6 and 14c, f, i, l). However, since this radial is located near the southernmost limit of the SEC bifurcation (~17°S) and is under the influence of the RCB topography (Fig. 3), the circulation over this region presents distinct patterns over the shelf and shelf-break/slope regions between seasons. During the spring/summer seasons, when a well organized southward flow occupies the first 100 m of the water depth (Fig. 14c, f), the circulation at the inner- and mid-shelves is southward oriented throughout the water column, presenting a remarkable vertical shear (Fig. 18b, c). The variability of the alongshore currents at the inner- and mid-shelf regions is mainly driven by the wind forcing (Table 4), with a correlation higher than 0.50. No significant coherence was observed with the oceanic region (Table 3). At the cross-shore direction, the surface currents show a significant out-of-phase correlation with the alongshore wind.

Table 3
Lagged cross-correlation functions between the sub-inertial alongshore depth-averaged currents at the inner-shelf, mid-shelf and shelf-break and the alongshore depth-averaged currents at the oceanic region at R10, R14 and R16 radials during the Spring/Summer and Autumn/Winter seasons. At the oceanic stations, the alongshore currents are depth-averaged from the surface to the depth of 150 m (R10), 80 m (R14) and 85 m (R16). Positive lags (in hours) indicate that the inner-shelf, mid-shelf or shelf-break currents lag the oceanic currents. See Figs. 3 and 14a for the geographic location of the stations.

Radial	Austral Station	Inner-shelf (cc/lag)	Mid-shelf (cc/lag)	Shelf-break (cc/lag)
R10	Spring/Summer	+0.47/−3	+0.56/0	+0.71/0
	Autumn/Winter	+0.45/−2	+0.59/0	+0.60/+2
R14	Spring/Summer	+0.30/−4	+0.50/0	+0.63/+1
	Autumn/Winter	+0.42/−2	+0.53/−1	+0.72/0
R16	Spring/Summer	+0.30/−3	+0.30/−1	+0.77/+4
	Autumn/Winter	+0.30/−3	+0.40/−2	+0.73/−1

At the shelf-break and oceanic regions, the alongshore currents show a pattern different to those observed at the inner and mid shelves. Here, although the currents are still southward oriented and present a moderate vertical shear (mainly at the shelf-break), they are very weak and highly variable near the bottom (Fig. 18d, e). This behaviour, associated with the high coherence ($\gamma^2 = 0.77$) between the depth-averaged currents (Table 3) and the low correlation between the alongshore currents and wind throughout

Table 4
Lagged cross-correlation functions between the sub-inertial alongshore wind and the alongshore (v) and cross-shore (u) components of the surface (S) and bottom or sub-surface (B) currents at the inner-shelf (IS), mid-shelf (MS), shelf-break (SB) and oceanic region (OR) at the R10, R14 and R16 radials during the Spring/Summer (S/S) and Autumn/Winter (A/W) seasons. The sub-surface currents at the OR are located at the depths of 150 m (R10), 80 m (R14) and 85 m (R16). Positive lags (hours) indicate that the currents lag the winds. See Figs. 3 and 14a for the geographic location of the stations.

	Wind x v current (cc/lag)				Wind x u current (cc/lag)			
Radial	IS	MS	SB	OR	IS	MS	SB	OR
R10								
S/S								
S	+0.62/1.8	+0.37/2.6	+0.30/3.5	+0.30/5.5	−0.70/0.8	−0.66/0.6	−0.60/0.2	−0.27/0.1
B	+0.28/1.9	+0.12/0.4	0/0	+0.30/3.4	+0.70/0.8	+0.27/0	+0.10/1.8	+0.10/0
A/W								
S	+0.64/1.3	+0.40/2.0	+0.34/3.3	+0.26/5.1	-0.62/0.6	-0.60/0.1	+0.60/0.1	+0.26/0.33
B	+0.45/1.8	+0.22/2.8	+0.10/3.0	+0.26/6.2	+0.63/0.83	+0.26/0	0/0	0/0
R14								
S/S								
S	+0.84/0.8	+0.52/1.5	+0.35/2.0	+0.15/0.8	+0.73/0.5	−0.24/0.22	−0.28/0	−0.11/0
B	+0.73/1.0	+0.30/2.0	+0.11/1.9	+0.10/1.9	+0.82/0.6	+0.68/1.0	+0.38/0.5	+0.30/1.0
A/W								
S	+0.87/0.6	+0.76/1.5	+0.61/1.7	+0.44/1.6	+0.84/0.5	+0.34/1.2	0/0	-0.27/0
B	+0.82/0.9	+0.68/1.7	+0.50/2.1	+0.38/2.1	+0.87/0.5	+0.73/1.2	+0.62/1.2	+0.18/1.0
R16								
S/S								
S	+0.54/0.7	+0.50/0.6	+0.38/0.3	+0.17/0	−0.50/1.7	−0.50/1.0	−0.28/1.0	−0.21/0.3
B	+0.48/1.0	+0.50/0.38	+0.17/.2	+0.18/2.9	−0.10/3.9	+0.33/0.6	−0.17/3.2	−0.14/3.2
A/W								
S	+0.78/0.8	+0.73/0.9	+0.47/0	+0.22/0	−0.57/2.0	−0.63/1.4	−0.46/1.0	−0.38/0.4
B	+0.72/0.9	+0.60/1.0	+0.30/1.5	+0.18/2.5	+0.42/2.7	−0.27/2.4	0/0	−0.20/3.3

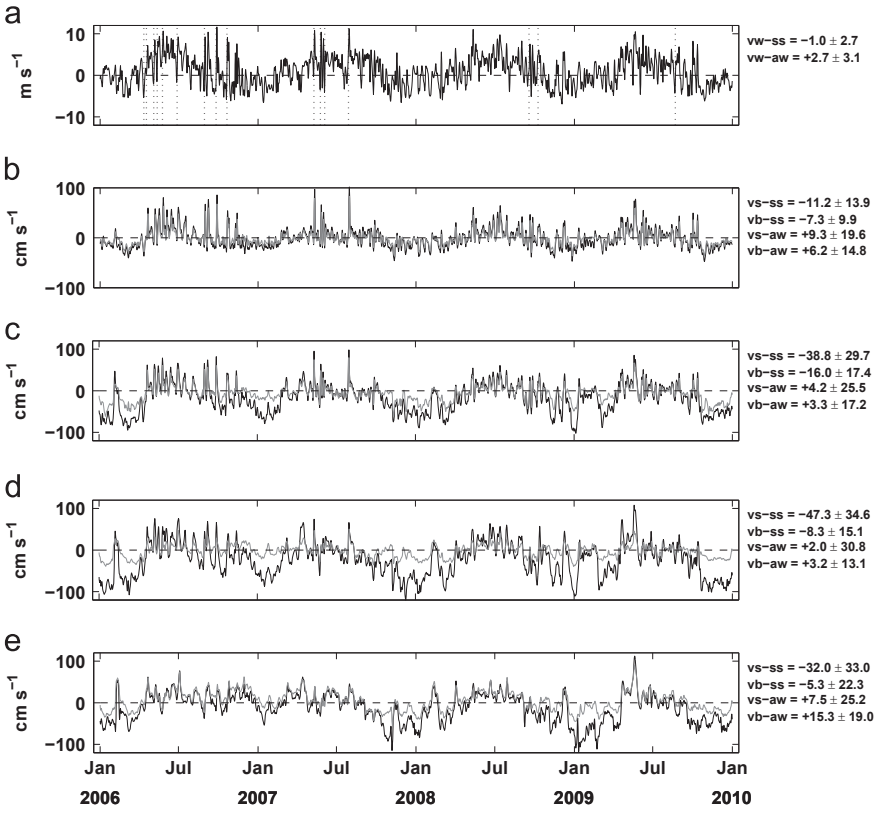

Fig. 17. Sub-inertial time-series (2006–2009) of the alongshore surface (black lines) and bottom/80 m (gray lines) currents at the (b) inner-shelf (IS), (c) mid-shelf (MS), (d) shelf-break (SB) and (e) oceanic region (OR) at radial R14. (a) The sub-inertial alongshore wind time-series derived from QuickSCAT for a point located close to the current time-series. The dotted vertical lines represent the cold-front passages (Inpe, 2011). The associated mean and standard deviation of the alongshore components of the wind (vw), and surface (vs) and bottom (vb) currents during the spring/summer (ss) and autumn/winter (aw) seasons are presented on the right side of the panels. The vertical axis is oriented in the N/S direction. See Figs. 3 and 14b for the geographic location of the stations.

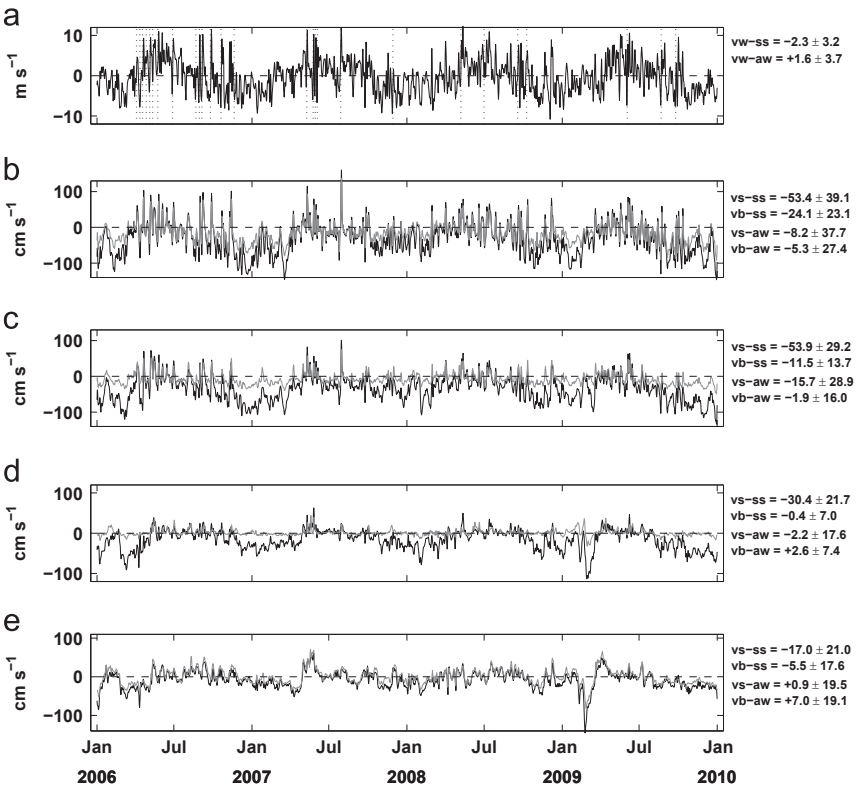

Fig. 18. Sub-inertial time-series (2006–2009) of the alongshore surface (black lines) and bottom/85 m (gray lines) currents at the (b) inner-shelf (IS), (c) mid-shelf (MS), (d) shelf-break (SB) and (e) oceanic region (OR) at radial R16. (a) The sub-inertial alongshore wind time-series derived from QuickSCAT for a point located close to the current time-series. The dotted vertical lines represent the cold-front passages (Inpe, 2011). The associated mean and standard deviation of the alongshore components of the wind (vw), and surface (vs) and bottom (vb) currents during the spring/summer (ss) and autumn/winter (aw) seasons are presented on the right side of the panels. The vertical axis is oriented in the N/S direction. See Figs. 3 and 14c for the geographic location of the stations.

the water column (Table 4), suggests an interaction of the alongshore flow with the WBC dynamics and the irregular RCB topography, constraining and altering the passing flow, as reported by Rezende et al. (2011).

4.3.2. *Autumn/winter scenario*

During the autumn/winter months, the northward NBUC at R10 increases and eventually occupies the shelf, as observed during July (Fig. 14j). As a consequence, the surface alongshore currents over the shelf are highly variable, with a weak mean southward component at the inner (-3.4 cm s^{-1}) and mid (-1.1 cm s^{-1}) shelves and a mean northward flow ($+8.0$ cm s^{-1}) at the shelf-break (Fig. 16b–d). The bottom currents along the shelf are more influenced by the flow over the slope, being more intense and less variable. The alongshore bottom currents at the slope region present a more stable pattern with a mean northward flow with intensity higher ($+46.1$ cm s^{-1}) than that observed for the mean surface flow ($+21.7$ cm s^{-1}). At the mid-shelf and shelf-break regions, the alongshore depth-averaged currents present a high correlation with those at the slope region ($\gamma^2 = 0.6$, Table 3). The response of the surface shelf currents to the wind forcing presents a similar pattern to that observed during the spring/summer seasons, with the highest (lowest) correlation of $\gamma^2 = 0.64$ ($\gamma^2 = 0.26$) at the inner-shelf (oceanic region).

In addition, the higher correlations between the alongshore component of the currents and wind at the inner- and mid-shelves (Table 4) show the effect of the less intense vertical stratification observed during the autumn/winter seasons. The cross-shore currents pattern at these regions, as observed for the spring/summer seasons, shows the effect of the Ekman transport, with surface (bottom) currents out-of-phase (in-phase) with the alongshore wind component.

At radial R14 a complete reversal of the mean flow is observed at the shelf and slope regions during the autumn/winter seasons, and the surface and bottom currents over the shelf present a strong variability when compared to the mean flow (Fig. 17b–d). This high variability can be related to: (i) the more frequent passage of cold frontal systems (Fig. 17a, vertical dotted lines); (ii) the fact that R14 is located in a region where the mean surface currents bifurcate into a northward and a southward flow (Fig. 6c, d) and (iii) the increased number of episodes when the NBUC occupies the shelf-break/slope regions (Fig. 14h, k), which reflect on the higher correlation with these currents with those at the oceanic region (Table 3). Although the variability of surface and bottom currents at the oceanic region is similar to those observed at mid-shelf and shelf-break, the mean flow is more intense and increases with depth, reflecting the presence of a more constant sub-surface northward flow of NBUC during the autumn/winter seasons.

Also, the alongshore currents over the radial R14 shelf present a stronger barotropic signal when compared with the spring/summer seasons, being well correlated with the wind forcing and reaching a correlation value of $\gamma^2 = 0.87$ at the inner-shelf (Table 4). In addition, and as observed during the spring/summer scenario, the low correlation and the negative phase relationship with the currents at the slope (Table 3) suggests that the wind is the main forcing mechanism for driving the shelf currents. At the cross-shore direction, the positive correlation with the wind forcing along depth indicates that the surface and bottom Ekman layers interact.

Following the southward excursion of the SEC bifurcation, which reaches its southernmost position (~17°S) in July, the

influence of the NBUC northward flow on the shelf circulation at radial R16 is more pronounced during the autumn/winter seasons (Fig. 14l) and, in addition, an intense mesoscale activity is observed over the RCB, with the presence of a surface anticyclonic circulation (Fig. 6). The mean surface circulation over the shelf is still southward oriented on the mean term, but highly variable (Fig. 18b–d), presenting a more stable flow toward the bottom at the inner-shelf region. At the inner- and mid-shelves, a low correlation between the alongshore depth-averaged currents and those at the oceanic region (Table 3) is observed. The high correlation along depth ($\gamma^2 > 0.60$) with the alongshore wind forcing (Table 4) indicates that the wind is still the main forcing mechanism of the circulation at these regions. At the cross-shore direction, only the surface cross-shore currents present a significant coherence with the alongshore wind.

At the shelf-break and slope regions of radial R16, the mean alongshore currents are mainly northward oriented and highly variable, with almost no vertical shear (Fig. 18d, e), reflecting the influence of the NBUC flow. In addition, the low correlation between the alongshore wind forcing with both alongshore and cross-shore currents (Table 4) and the high correlation ($\gamma^2 = 0.73$) between the depth-averaged alongshore currents (Table 3), highlight the influence of the dynamics associated with the WBC on the circulation at these regions.

5. Summary

The EBS is a passive tropical margin which dynamics is strongly influenced by the seasonal latitudinal excursion of the SEC bifurcation and by the large scale seasonality of the trade winds, both influenced by the north–south displacement of the ITCZ. To investigate the EBS seasonal circulation and its interaction with the WBC flowing along the slope, a regional ocean model was implemented and configured with a refined grid (1/36°) and realistic forcings (6-hourly winds and surface fluxes, daily large scale oceanic forcing and tides). The model proved to be suitable and reliable to study the circulation within the EBS, since it was able to capture the available observed data with a reasonable representation of the main features.

The model results show, based on the cross-shore radials used for the analysis, that for the northern limit (radial R10 located at 10°S) and for the TW layer (first 150 m of the water column) the northward flow is the dominant pattern with an annual transport of +2.41 Sv. The southward flow appears as a thin flow confined to the top 50 m of the water column during the spring/summer seasons, with an annual transport of −0.48 Sv. For the SACW layer (~150–400 m), the northward flow reaches an annual transport of +7.84 Sv and the southward flow nearly vanishes, being associated with only −0.28 Sv of the annual net transport. While the surface circulation at the inner- and mid-shelves at R10 radial is more influenced by the wind forcing, at the shelf-break the currents are mainly driven by the slope circulation during all seasons. During the autumn/winter scenario, when the SEC bifurcation reaches its southernmost position, the bottom currents along the shelf are more influenced by the northward flow over the slope, being more intense and less variable than the surface currents.

At the middle (radial R14 located at 14°S) and southern (radial R16 located at 16°S) domain, there is an alternate dominance of the southward/northward flow for the first 150 m of the water column, with the dominance of the southward (northward) flow between October and February (March and September) months at radial R14. However, the annual net transport of −0.07 Sv (−0.47 Sv) at R14 (R16) is southward oriented. On the other hand, at the SACW layer (~150–400 m), the annual net transport of +4.53 Sv (+2.90 Sv) at R14 (R16) is northward oriented and the dominance of the northward flow is clear. During the spring/summer scenario, the circulation at the first 150 m at the radial R14 is well defined southwards and, while at the inner-shelf it is mainly driven by the remote wind forcing, at the mid-shelf both the wind and the flow over the slope act to drive these currents. For this scenario, the currents at the shelf-break are more influenced by the currents at the slope, and, at both regions, the bottom currents present low mean intensity and high variability, which could be a response to the opposing southward/northward flows, that can eventually interact. During the autumn/winter scenario, a complete reversal of the mean flow is observed along the shelf and slope regions at R14. The currents throughout the water column increase their variability when compared to the mean flow, possibly due to the increased number of episodes when the northward flow occupies the shelf. Nonetheless, a significant influence of the wind at the shelf region is still observed. The currents at the inner-shelf during this scenario are mainly wind driven, as observed for the spring/summer scenario.

At the southern limit (radial R16 located at 16°S), a permanent southward flow over the shelf and a marked mesoscale activity is observed throughout the year, and the region presents different contribution of the forcing mechanisms at the shelf and shelf-break/slope regions. During the spring/summer scenario, when the SEC bifurcation reaches its northernmost position (~13°S), a well defined southward flow at the top 100 m is present and a considerable vertical shear over the shelf is observed. However, while the circulation at the inner- and mid-shelves is mainly wind driven, at the shelf-break/slope it presents a poor correlation with the wind forcing and a strong influence of the WBC dynamics. The currents are indeed very weak and highly variable near the bottom. During the autumn/winter scenario, when the SEC bifurcation reaches its southernmost position (~17°S), the region experiences a similar dominance of the southward/northward flow at the top 150 m depth in comparison to the spring/summer scenario. As a response, a decrease of the southward (northward) flow over the shelf (slope) occurs. In this scenario, the circulation over the shelf presents a less intense vertical shear, but, while at the inner- and mid-shelves it is southward oriented and highly correlated with the wind forcing, presenting no contribution of the currents over the slope, at the shelf-break/slope, the depth-averaged currents are highly correlated, being mainly northward oriented. This pattern, associated with the low correlation with the wind forcing, enhances the influence of the WBC dynamics at these regions.

Acknowledgements

This research was supported by PETROBRAS and approved by the Brazilian oil regulatory agency ANP (Agência Nacional de Petróleo, Gás Natural e Biocombustíveis), within the special participation research project Oceanographic Modeling and Observation Network (REMO). Fabiola N. Amorim was supported by Brazilian scholarships from CAPES and REMO. Mauro Cirano and Edmo J.D. Campos were supported by CNPq Research grants.

References

Allen, J.S., Beardsley, R.C., Blanton, J.O., Biocourt, W.C., Butman, B., Coachman, L.K., Huyer, A., Kinder, T.H., Royer, T.C., Shumacher, J.D., Smith, R.L., Strurges, W., 1983. Physical oceanography of continental shelves. Reviews of Geophysics and Space Physics 21 (5), 1149–1181.

Amorim, F.N., Cirano, M., Soares, I.D., Campos, E.J.D., Middleton, J., 2012. The influence of large-scale circulation and transient processes on the seasonal circulation at Eastern Brazilian Shelf, near 13°S. Continental Shelf Research 32, 47–61, http://dx.doi.org/10.1016/j.csr.2011.10.011.

Amorim, F.N., Cirano, M., Soares, I.D., Lentini, C.A.D., 2011. Coastal and shelf circulation in the vicinity of Camamu Bay (14°S), Eastern Brazilian Shelf.

Continental Shelf Research 31, 108–119, http://dx.doi.org/10.1016/j.csr.2010.11.011.
AVISO, 2011. SSALTO/DUACS User Handbook: (M)SLA and (M)ADT Near-Real Time and Delayed Time Products. Technical Report, Centre National D'études Spatiales, CLS-DOS-NT-06-034-Issue 2.4, 49 pp.
Barth, A., Alvera-Azcárate, A., Weisberg, R.H., 2008. Benefit of nesting a regional model into a large-scale ocean model instead of climatology. Application to the West Florida Shelf. Continental Shelf Research 28 (4–5), 561–573.
Campos, E.J.D., Velhote, D., Silveira, I.C.A., 2000. Shelf break upwelling driven by Brazil Current cyclonic meanders. Geophysical Research Letters 27 (6), 751–754.
Castro, B.M., Miranda, L.B., 1998. Physical oceanography of the Western Atlantic continental shelf located between 4°N and 34°S coastal segment (4, *W*). In: Robinson, A.R., Brink, K.H. (Eds.), The Sea, vol. 11. Wiley, pp. 209–251.
Chapman, D., 1985. Numerical treatment of cross-shelf open boundaries in a barotropic coastal ocean model. Journal of Physical Oceanography 15, 1060–1075.
Cirano, M., Mata, M.M., Campos, E.J.D., Deiró, N., 2006. A circulação oceânica de larga-escala na região oeste do Atlântico Sul: validação da climatologia anual com base no modelo de circulação global OCCAM. Revista Brasileira de Geofísica 24, 209–230.
Dominguez, J.M.L., 2006. The Coastal Zone of Brazil—an overview. Journal of Coastal Research 39 (special issue), 16–20.
Egbert, G.D., Erofeeva, S.Y., 2002. Efficient inverse modeling of barotropic ocean tides. Journal of Atmospheric and Oceanic Technology 19 (2), 183–204.
FEMAR, 2011. Estações maregráficas ⟨http://www.fundacaofemar.org.br/⟩.
Flather, R., 1976. A tidal model of the northwest European continental shelf. Mémoires de la Societe Royale des Sciences de Liège 6 (10), 141–164.
GLOBE Task Team, 1999. The Global Land One-kilometer Base Elevation (GLOBE) Digital Elevation Model, version 1.0. Technical Report, NOAA-NGDC ⟨http://www.ngdc.noaa.gov/mgg/topo/globe.html⟩.
Haidvogel, D.B., Arango, H., Budgell, W.P., Cornuelle, B.D., Curchitser, E., Di Lorenzo, E., Fennel, K., Geyer, W.R., Hermman, A.J., Lanerolle, L., Levin, J., McWilliams, J.C., Miller, A.J., Moore, A.M., Powell, T.M., Shchepetkin, A.F., Sherwood, C.R., Signell, R.P., Warner, J.C., Wilkin, J., 2008. Ocean forecasting in terrain-following coordinates: formulations and skill assessment of the Regional Ocean Modeling System. Journal of Computational Physics 227, 3595–3624.
Haidvogel, D.B., Beckmann, A., 1999. Numerical Ocean Circulation Modeling. Series on Environmental Science and Management, vol. 2. Imperial College Press.
HYCOM, 2011. Consortium for Data Assimilative Modeling—HYCOM+NCODA Global 1/12° Analysis. Available at ⟨http://www.hycom.org/dataserver/glb-analysis/⟩.
IFREMER, 2011. Near Real Time Blended Surface Winds. Technical Report, Center for Satellite Exploitation and Research—CERSAT ⟨http://cersat.ifremer.fr/data/discovery/by_product_type/gridded_products/mwf_blended⟩.
Inpe, C., 2011. Climanálise - boletim de monitoramento e análise climática, vols. 21 and 22. ⟨http://www6.cptec.inpe.br/revclima/boletim/⟩.
Kanamitsu, M., Ebisuzaki, W., Woollen, J., Yang, S.K., Hnilo, J.J., Fiorino, M., Potter, G.L., 2002. NCEP-DOE AMIP-II reanalysis R-2. Bulletin of the American Meteorological Society 83, 1631–1643.
Knoppers, B., Ekau, W., Figueiredo, A.G., 1999. The coast and shelf of east and northeast Brazil and material transport. Geo-Marine Letters 19 (3), 171–178, http://dx.doi.org/10.1007/s003670050106.
Leão, Z., 2002. Abrolhos - o complexo recifal mais extenso do oceano Atlântico Sul. In: Schobbenhaus, C., Campos, D., Queiroz, E., Winge, M., Berbert-born, M. (Eds.), Sítios Geológicos e Paleontológicos do Brasil, vol. 1. DNPM, pp. 345–359.
Lee, T.N., Ho, W.J., Kourafalou, V., Wang, J.D., 1984. Circulation on the continental shelf of the Southeastern United States. Part i: subtidal response to wind and gulf stream forcing during winter. Journal of Physical Oceanography 14, 1001–1012.
Lessa, G., Dominguez, J.M.L., Bittencourt, A.C.S.P., Brichta, A., 2001. The tides and tidal circulation of Todos os Santos Bay, Northeast Brazil: a general characterization. Anais da Academia Brasileira de Ciências 73 (2), 245–261.
Marchesiello, P., McWilliams, J.C., Shchepetkin, A., 2001. Open boundary conditions for long-term integration of regional oceanic models. Ocean Modelling 3, 1–20.
Marta-Almeida, M., Hetland, R.D, Zhang, X., 2013. Evaluation of model nesting performance on the Texas-Lousiana continental shelf. Journal of Geophysical Research 118, http://dx.doi.org/10.1002/jgrc.20163.
Olavo, G., Costa, P.A.S., Martins, A., Ferreira, B.P., 2011. Shelf-edge reefs as priority areas for conservation of reef fish diversity in the tropical Atlantic. Aquatic Conservation: Marine and Freshwater Ecosystems 21, 199–209.
Orfanidis, S.J., 1998. Optimum Signal Processing. An Introduction, second ed.. Macmillan.
Pawlowicz, R., Beardsley, B., Lentz, S., 2002. Classical tidal harmonic analysis including error estimates in MATLAB using t_tide. Computers & Geosciences 28, 929–937.
Penven, P., Debreu, L., Marchesiello, P., McWilliams, J.C., 2006. Evaluation and application of the ROMS 1-way embedding procedure to the Central California upwelling system. Ocean Modelling 12, 157–187.
Pereira, A., Belem, A., Castro, B.M., Geremias, R., 2005. Tide–topography interaction along the eastern Brazilian shelf. Continental Shelf Research 25, 1521–1539.
Rezende, L.F., Silva, P.A., Cirano, M., Peliz, A., Dubert, J., 2011. Mean circulation, seasonal cycle and eddy interactions in the Eastern Brazilian Margin, a nested ROMS model. Journal of Coastal Research 27 (2), 329–347.
Rodrigues, R.R., Rothstein, L.M., Wimbush, M., 2007. Seasonal variability of the south equatorial current bifurcation in the Atlantic Ocean: a numerical study. Journal of Physical Oceanography 37, 16–30.
Schott, F.A., Brandt, P., Hamann, M., Fischer, J., Stramma, L., 2002. On the boundary flow off Brazil at 5–10°S and its connection to the interior tropical Atlantic. Geophysical Research Letters 29 (17), 21–1/4.
Schott, F.A., Dengler, M., Zantopp, R., Stramma, L., Fischer, J., Brandt, P., 2005. The shallow and deep western boundary circulation of the South Atlantic at 5°–11°S. Journal of Physical Oceanography 35, 2031–2053.
Schott, F.A., Fischer, J., Stramma, L., 1998. Transports and pathways of the upper-layer circulation in the western tropical Atlantic. Journal of Physical Oceanography 28 (10), 1904–1928.
Shchepetkin, A.F., McWilliams, J.C., 2003. A method for computing horizontal pressure-gradient force in an oceanic model with a non-aligned vertical coordinate. Journal of Geophysical Research 108, 1–34.
Shchepetkin, A.F., McWilliams, J.C., 2005. The regional oceanic modeling systems (ROMS): a split-explicit, free-surface, topography-following-coordinate oceanic model. Ocean Modelling 9, 347–404.
Silva, M., Araujo, M., Servain, J., Penven, P., Lentini, C.A.D., 2009. High-resolution ocean dynamics simulation in the southwestern tropical Atlantic. Ocean Modelling 30, 256–269.
Silveira, I.C.A., Miranda, L.B., Brown, W.S., 1994. On the origins of the North Brazil Current. Journal of Geophysical Research 99 (November), 22501–22512.
Silveira, I.C.A., Schmidt, A.C.K., Campos, E.J.D., Godoi, S.S., Ikeda, Y., 2000. A Corrente do Brasil ao largo da costa leste Brasileira. Revista Brasileira de Geofísica 48 (2), 171–183.
Soares, I.D., Moller, O.J., 2001. Low-frequency and water mass spacial distribution on the Southern Brazilian shelf. Continental Shelf Research 21, 1785–1814.
Soutelino, R.G., Silveira, I.C.A., Gangopadhyay, A., Miranda, J.A., 2011. Is the Brazil current eddy-dominated to the north of 20°S? Geophysics Research Letters 38 (L03607), http://dx.doi.org/10.1029/2010GL046276.
Stramma, L., England, M., 1999. On the water masses and mean circulation of the South Atlantic Ocean. Journal of Geophysical Research 104 (C9), 20863–20883.
Stramma, L., Ikeda, Y., Peterson, R.G., 1990. Geostrophic transport in the Brazil current region North of 20°S. Deep-Sea Research 37 (12), 1875–1886.
Stramma, L., Schott, F., 1999. The mean flow field of the tropical Atlantic Ocean. Deep-Sea Research, Part II 46, 279–303.
Veleda, D., Araujo, M., Zantopp, R., Montagne, R., 2012. Intraseasonal variability of the North Brazil Undercurrent forced by remote winds. Journal of Geophysical Research C11024 10 p.
Veleda, D.R.A., Araujo, M., Silva, M., Montagne, R., Araújo, R., 2011. Seasonal and interannual variability of the southern South Equatorial current bifurcation and meridional transport along the eastern Brazilian edge. Tropical Oceanography, 27–59, Online ISNN: 1679–3013.
Walters, R.A., Heston, C., 1982. Removing tidal-period variations from time-series data using low-pass digital filters. Journal of Physical Oceanography 12, 112–115.
Zhang, X., Hetland, R.D., Marta-Almeida, M., DiMarco, S.F, 2012. A numerical investigation of the Mississippi and Atchafalaya freshwater transport, filling and flushing times on the Texas-Louisiana shelf. Journal of Geophysical Research 117 (C11009), http://dx.doi.org/10.1029/2012JC008108.